JOURNAL OF MATERIALS SCIENCE 24 (1989) 761–783

Review
Flexible composites

TSU-WEI CHOU
Center for Composite Materials, and Department of Mechanical Engineering, University of Delaware, Newark, Delaware 19716, USA

This paper reviews the linear and non-linear elastic behaviour of flexible composites, which are based on elastomeric polymers and exhibit a usable range of deformation much larger than those of conventional thermosetting or thermoplastic polymer-based composites. The types of flexible composites examined are cord/rubber composites, coated fabrics and composites containing wavy fibres. The classical lamination theory forms the basis of analysing the linear elastic behaviour. Three analytical approaches have been developed for predicting the non-linear elastic behaviour. The advancement in the predicability of analytical models enhances the utilization of flexible composites as load-bearing structural composites. The versatility of flexible composites in engineering applications lies in the fact that their load–deformation behaviour can be tailored by suitable selection of fibre/matrix systems and the design of fibre geometric configuration.

1. Introduction

The term "flexible composites" is used here to identify composites based upon elastomeric polymers of which the usable range of deformation is much larger than those of the conventional thermosetting or thermoplastic polymer-based composites. The ability of flexible composites to sustain large deformation and fatigue loading, and still provide high load-carrying capacity has been mainly analysed in pneumatic tyre and conveyor belt constructions. However, the unique capability of flexible composites is yet to be explored and investigated. The real potential of flexible composites can be assessed only if their fundamental characteristics are understood [1, 2].

Besides tyres and conveyor belts, flexible composites can be found in a wide range of applications. Coated (with PVC, Teflon, rubber, etc.) fabrics have been used for air or cable-supported building structures, tents, parachutes, decelerators in high-speed aeroplanes, bullet-proof vests, tarpaulin, inflated structures such as boats and escape slides, safety nets, and other inexpensive products. Hoses, flexible diaphragms, racket strings, surgical replacements, geotextiles, and reinforced membrane structures, in general, are examples of flexible composites.

The purpose of this review article is to assess the state of knowledge in terms of modelling and predicting the elastic behaviour of flexible composites. Three categories of materials are examined: pneumatic tyres, coated fabrics, and flexible composites containing wavy fibres; they provide the model systems of analysis with elastic behaviour ranging from small to large deformations. Further justifications for the studies of these three systems are given below.

The performance characteristics of pneumatic tyres are primarily controlled by the anisotropic properties of the cord/rubber composite. The low-modulus, high-elongation rubber contains the air and provides abrasion resistance and road grip. The high-modulus, low-elongation cords carry most of the loads applied to the tyre in service [3]. According to Walter [3], the first quantitative study of cord/rubber elastic properties, in the tyre industry, was published in Germany in 1939 by Martin [4] who analysed bias-ply aircraft tyres using thin shell theory to approximate toroidal tyre behaviour. Martin's analysis of the orthotropic composite elastic constants assumes that the fibres are inextensible and the matrix stiffness is negligibly small; this approach has been referred to herein as the classical netting analysis. Studies of the cord/rubber properties became active worldwide in the 1960s as represented by the work of Clark [5–7] in the USA, Gough [8, 9] in Great Britain, Akasaka [10] in Japan, and Biderman and co-workers [11] in the Soviet Union.

It should be noted that the existing analysis on tyre mechanics is primarily based upon the well-developed anisotropic theory of rigid laminated composites for small linear elastic deformation. Thus, the problems of viscoelasticity, strength behaviour, fatigue and large non-linear behaviour are often ignored.

In the case of coated fabrics, limited attention has been given to the material stress–strain response to arbitrary loading paths and histories. Experimental studies of the biaxial stress–strain behaviour can be found in the works of Alley and Fairson [12], Reindhardt [13], and Skelton [14]. Attempts have also been made by Stubbs and Thomas [15], and Akasaka and Yoshida [16] to analytically model the elastic and inelastic properties of coated fabrics under biaxial loading. Some of these results are briefly recapitulated in this review.

0022–2461/89 $03.00 + .12

The third and last part of this review focus on the understanding of the large non-linear deformation of flexible composites. To this end, model material systems for analytical purpose, need to be identified. The large non-linear deformation could originate from two sources, i.e. matrix and fibre. In order to realize fully the ability of the elastomeric matrix to sustain large deformation, the fibres must be able to deform accordingly with the matrix. This can be achieved by (a) using short fibres, (b) arranging continuous fibres in such an orientation that they are allowed to rotate as the load increases, and (c) using reinforcements in woven, knitted, braided, or other wavy forms [1].

Possibility (c) is particularly interesting in that it utilizes the waviness of the fibres. The gradual straightening of the wavy fibres under external loading results in enhanced stiffness with increase in deformation. The linear and non-linear elastic behaviour of two- and three-dimensional textile structural composites has been examined by Chou and co-workers [17–19]. However, the analysis was based on small deformation theory. Thus, in the third part of this paper, a review of the non-linear finite deformation analysis of flexible composites is presented.

2. Basics of anisotropic laminate theory

The purpose of this section is briefly to outline the stress–strain relations for laminated composites. These constitutive relations based on the classical lamination theory are the basis for some of the analysis presented in this paper. The lamination theory is a relatively mature subject; its treatment can be found in text books of, for instance, Ashton *et al.* [20], Vinson and Chou [21], Jones [22], Tsai and Hahn [23], and Carlsson and Pipes [24].

2.1. Stress–strain relations for unidirectional laminae

A unidirectional lamina can be treated as an orthotropic material. Four independent constants are needed to specify its elastic behaviour. These constants, referring to the fibre (x_1) and transverse (x_2) directions, are denoted by E_1 (longitudinal Young's modulus), E_2 (transverse Young's modulus), ν_{12} (Poisson's ratio due to loading in the x_1 direction and contraction in the x_2 direction), and G_{12} (in-plane shear modulus). The relationship between these orthotropic elastic properties and the elastic properties of the fibre and matrix materials and the fibre volume fraction can be found using techniques well developed in the composite literature. Let the isotropic properties of the fibre and matrix be denoted by E (Young's modulus), ν (Poisson's ratio), G (shear modulus) and K (bulk modulus). Volume fractions are denoted by V, and the subscripts f and m indicate fibre and matrix, respectively. The following relations due to Hashin and Rosen, and reviewed by Rosen [25] are quoted for their concise forms and hence, ease in application.

$$E_1 = E_f V_f + E_m V_m + \frac{4V_f V_m(\nu_f - \nu_m)^2}{(V_m/K_f) + (V_f/K_m) + (1/G_m)} \quad (1)$$

$$E_2 = (4K_t^* G_t^*)\Big/\left[K_t^* + G_t^*\left(1 + \frac{4K_t^* \nu_{12}^2}{E_1}\right)\right] \quad (2)$$

$$\nu_{12} = \nu_f V_f + \nu_m V_m + \left[V_f V_m(\nu_f - \nu_m)\left(\frac{1}{K_m} - \frac{1}{K_f}\right)\right]\Big/\left(\frac{V_m}{K_f} + \frac{V_f}{K_m} + \frac{1}{G_m}\right) \quad (3)$$

$$G_{12} = G_m \frac{V_m G_m + (1 + V_f)G_f}{(1 + V_f)G_m + V_m G_f} \quad (4)$$

where

$$K_t^* = \frac{K_m K_f + (V_f K_f + V_m K_m)G_m}{V_m K_f + V_f K_m + G_m} \quad (5)$$

$$G_t^* = G_m \frac{(\alpha + \beta_m V_f)(1 + \varrho V_f^3) - 3V_f V_m^2 \beta_m^2}{(\alpha - V_f)(1 + \varrho V_f^3) - 3V_f V_m^2 \beta_m^2} \quad (6)$$

$$\alpha = (\gamma + \beta_m)/(\gamma - 1) \quad (7)$$

$$\beta = 1/(3 - 4\gamma) \quad (8)$$

$$\varrho = (\beta_m - \gamma\beta_f)/(1 + \gamma\beta_f) \quad (9)$$

$$\gamma = G_f/G_m \quad (10)$$

It should be noted that Equations 1 to 10 are actually for a unidirectional composite treated as a three-dimensional, transversely isotropic material. Five independent elastic constants are needed to describe such properties. K_t^* and G_t^* in Equations 5 and 6 are respectively, the transverse plane-strain bulk modulus and transverse shear modulus, of the unidirectional composite. For completeness, the transverse Poisson's ratio is given by

$$\nu_t^* = \frac{1}{2}\left(\frac{E_2}{G_t^*}\right) - 1 \quad (11)$$

The strain–stress relations for the unidirectional lamina in a plane stress state, referring to the x_1–x_2 plane, is given by

$$\begin{pmatrix} \varepsilon_1 \\ \varepsilon_2 \\ \gamma_{12} \end{pmatrix} = \begin{pmatrix} S_{11} & S_{12} & 0 \\ S_{12} & S_{22} & 0 \\ 0 & 0 & S_{66} \end{pmatrix} \begin{pmatrix} \sigma_1 \\ \sigma_2 \\ \tau_{12} \end{pmatrix} \quad (12)$$

Here, ε and σ denote the normal strain and stress components, respectively; γ and τ are the shear strain and stress, respectively. Again, x_1 and x_2 refer to the fibre and transverse directions, respectively. The elastic compliance constants S_{ij} in Equation 12 can be expressed in terms of the unidirectional lamina properties (often referred to as the engineering constants).

$$S_{11} = \frac{1}{E_1} \qquad S_{22} = \frac{1}{E_2} \quad (13)$$

$$S_{12} = -\frac{\nu_{12}}{E_1} = -\frac{\nu_{21}}{E_2} \quad (14)$$

$$S_{66} = \frac{1}{G_{12}} \quad (15)$$

Obviously the reciprocity of S_{12} holds. Four independent constants appear in Equation 12 and the lamina is termed especially orthotropic.

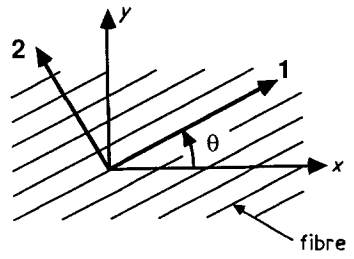

Figure 1 Fibre axis at an angle θ from the lamina reference axis.

Equation 12 can be inverted to obtain the stress–strain relations.

$$\begin{pmatrix}\sigma_1\\ \sigma_2\\ \tau_{12}\end{pmatrix} = \begin{pmatrix}Q_{11} & Q_{12} & 0\\ Q_{12} & Q_{22} & 0\\ 0 & 0 & Q_{66}\end{pmatrix}\begin{pmatrix}\varepsilon_1\\ \varepsilon_2\\ \gamma_{12}\end{pmatrix} \quad (16)$$

where the Q_{ij} are known as the reduced stiffness, and are related to the engineering constants of the unidirectional lamina as follows

$$Q_{11} = \frac{E_1}{1 - \nu_{12}\nu_{21}} \quad (17)$$

$$Q_{12} = \frac{\nu_{12}E_2}{1 - \nu_{12}\nu_{21}} = \frac{\nu_{21}E_1}{1 - \nu_{12}\nu_{21}} \quad (18)$$

$$Q_{22} = \frac{E_2}{1 - \nu_{12}\nu_{21}} \quad (19)$$

$$Q_{66} = G_{12} \quad (20)$$

It is worth noting that the engineering constants can also be expressed in terms of the reduced stiffness as

$$E_1 = Q_{11} - \frac{Q_{12}^2}{Q_{22}} \quad (21)$$

$$E_2 = Q_{22} - \frac{Q_{12}^2}{Q_{11}} \quad (22)$$

$$\nu_{12} = \frac{Q_{12}}{Q_{22}} \quad (23)$$

$$G_{12} = Q_{66} \quad (24)$$

For a unidirectional lamina situated at an angle θ with respect to the reference axes x–y (Fig. 1), the stress–strain relations in the x–y coordinates are

$$\begin{pmatrix}\sigma_x\\ \sigma_y\\ \tau_{xy}\end{pmatrix} = \begin{pmatrix}\boldsymbol{Q}_{11} & \boldsymbol{Q}_{12} & \boldsymbol{Q}_{16}\\ \boldsymbol{Q}_{12} & \boldsymbol{Q}_{22} & \boldsymbol{Q}_{26}\\ \boldsymbol{Q}_{16} & \boldsymbol{Q}_{26} & \boldsymbol{Q}_{66}\end{pmatrix}\begin{pmatrix}\varepsilon_x\\ \varepsilon_y\\ \gamma_{xy}\end{pmatrix} \quad (25)$$

where $\boldsymbol{Q}_{ij}$, the transformed reduced stiffnesses, are given by

$$\boldsymbol{Q}_{11} = Q_{11}\cos^4\theta + 2(Q_{12} + 2Q_{66})\sin^2\theta\cos^2\theta + Q_{22}\sin^4\theta \quad (26)$$

$$\boldsymbol{Q}_{12} = (Q_{11} + Q_{22} - 4Q_{66})\sin^2\theta\cos^2\theta + Q_{12}(\sin^4\theta + \cos^4\theta) \quad (27)$$

$$\boldsymbol{Q}_{22} = Q_{11}\sin^4\theta + 2(Q_{12} + 2Q_{66})\sin^2\theta\cos^2\theta + Q_{22}\cos^4\theta \quad (28)$$

$$\boldsymbol{Q}_{16} = (Q_{11} - Q_{12} - 2Q_{66})\sin\theta\cos^3\theta + (Q_{12} - Q_{22} + 2Q_{66})\sin^3\theta\cos\theta \quad (29)$$

$$\boldsymbol{Q}_{26} = (Q_{11} - Q_{12} - 2Q_{66})\sin^3\theta\cos\theta + (Q_{12} - Q_{22} + 2Q_{66})\sin\theta\cos^3\theta \quad (30)$$

$$\boldsymbol{Q}_{66} = (Q_{11} + Q_{22} - 2Q_{12} - 2Q_{66})\sin^2\theta\cos^2\theta + Q_{66}(\sin^4\theta + \cos^4\theta) \quad (31)$$

The unidirectional lamina referred to the x–y axes is termed generally orthotropic.

Equation 25 can be inverted to obtain the strain–stress relations in the following general form

$$\begin{pmatrix}\varepsilon_x\\ \varepsilon_y\\ \gamma_{xy}\end{pmatrix} = \begin{pmatrix}\boldsymbol{S}_{11} & \boldsymbol{S}_{12} & \boldsymbol{S}_{16}\\ \boldsymbol{S}_{12} & \boldsymbol{S}_{22} & \boldsymbol{S}_{26}\\ \boldsymbol{S}_{16} & \boldsymbol{S}_{26} & \boldsymbol{S}_{66}\end{pmatrix} = \begin{pmatrix}\sigma_x\\ \sigma_y\\ \tau_{xy}\end{pmatrix} \quad (32)$$

in which the $\boldsymbol{S}_{ij}$ are the transformed compliance constants and their relation to S_{ij} and θ are

$$\boldsymbol{S}_{11} = S_{11}\cos^4\theta + (2S_{12} + S_{66})\sin^2\theta\cos^2\theta + S_{22}\sin^4\theta \quad (33)$$

$$\boldsymbol{S}_{12} = S_{12}(\sin^4\theta + \cos^4\theta) + (S_{11} + S_{22} - S_{66})\sin^2\theta\cos^2\theta \quad (34)$$

$$\boldsymbol{S}_{22} = S_{11}\sin^4\theta + (2S_{12} + S_{66})\sin^2\theta\cos^2\theta + S_{22}\cos^4\theta \quad (35)$$

$$\boldsymbol{S}_{16} = (2S_{11} - 2S_{12} - S_{66})\sin\theta\cos^3\theta - (2S_{22} - 2S_{12} - S_{66})\sin^3\theta\cos\theta \quad (36)$$

$$\boldsymbol{S}_{26} = (2S_{11} - 2S_{12} - S_{66})\sin^3\theta\cos\theta - (2S_{22} - 2S_{12} - S_{66})\sin\theta\cos^3\theta \quad (37)$$

$$\boldsymbol{S}_{66} = 2(2S_{11} + 2S_{22} - 4S_{12} - S_{66})\sin^2\theta\cos^2\theta + S_{66}(\sin^4\theta + \cos^4\theta) \quad (38)$$

The engineering constants of the unidirectional lamina referring to the x–y axes, which are not aligned with the material principal directions, can be expressed as functions of the off-axis angle, θ, by using Equations 13 to 15 and 33 to 38

$$\frac{1}{E_x} = \frac{1}{E_1}\cos^4\theta + \left(\frac{1}{G_{12}} - \frac{2\nu_{12}}{E_1}\right)\sin^2\theta\cos^2\theta + \frac{1}{E_2}\sin^4\theta \quad (39)$$

$$\nu_{xy} = E_x\left(\frac{\nu_{12}}{E_1}(\sin^4\theta + \cos^4\theta) - \left(\frac{1}{E_1} + \frac{1}{E_2} - \frac{1}{G_{12}}\right)\sin^2\theta\cos^2\theta\right) \quad (40)$$

$$\frac{1}{E_y} = \frac{1}{E_1}\sin^4\theta + \left(\frac{1}{G_{12}} - \frac{2\nu_{12}}{E_1}\right)\sin^2\theta\cos^2 + \frac{1}{E_2}\cos^4\theta \quad (41)$$

$$\frac{1}{G_{xy}} = 2\left(\frac{2}{E_1} + \frac{2}{E_2} + \frac{4\nu_{12}}{E_1} - \frac{1}{G_{12}}\right)\sin^2\theta\cos^2\theta + \frac{1}{G_{12}}(\sin^4\theta + \cos^4\theta) \quad (42)$$

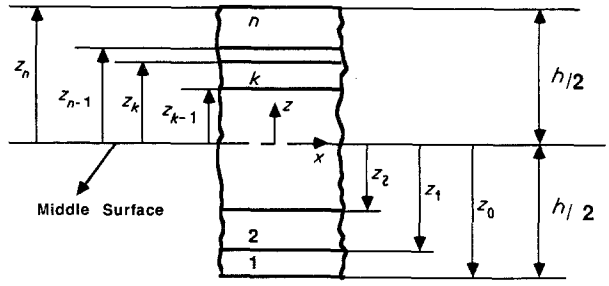

Figure 2 An n-layered laminate.

2.2. Classical lamination theory

Based upon the constitutive relations for a lamina composed of a generally orthotropic material, Equation 25, the constitutive relations for a laminate formed by bonding several laminae together is presented in this section. The orientation and material system of each lamina are general. Fig. 2 depicts the geometry of an n-layered laminate of thickness h; the x–y plane coincides with the laminate geometric middle plane. Following the approach of the classical, linear, thin-plate theory, the following assumptions are made [21].

1. A lineal element of the plate extending through the plate thickness, normal to the middle surface (x–y plane) in the unstressed state, upon the application of load: (a) undergoes at most a translation and a rotation with respect to the original coordinate system, and (b) remains normal to the deformed middle surface. This assumption implies that the lineal element does not elongate or contract, and remains straight upon load applications.

2. The plate resists lateral and in-plane loads by bending, transverse shear stress, and in-plane action, not through block-like compression or tension in the plate in the thickness direction.

Based upon the foregoing assumptions, also known as the Kirchhoff hypothesis for plates, the strain components can be derived

$$\begin{pmatrix} \varepsilon_x \\ \varepsilon_y \\ \gamma_{xy} \end{pmatrix} = \begin{pmatrix} \varepsilon_x^0 \\ \varepsilon_y^0 \\ \gamma_{xy}^0 \end{pmatrix} + z \begin{pmatrix} \kappa_x \\ \kappa_y \\ \kappa_{xy} \end{pmatrix} \tag{43}$$

Here, ε_x^0, ε_y^0 and γ_{xy}^0 are the laminate middle plane strain, which are expressed in terms of the middle plane displacements u_0 and v_0

$$\varepsilon_x^0 = \frac{\partial u_0}{\partial x}, \quad \varepsilon_y^0 = \frac{\partial v_0}{\partial y}, \quad \gamma_{xy} = \frac{\partial u_0}{\partial y} + \frac{\partial v_0}{\partial x} \tag{44}$$

The middle plane curvatures are related to the z-direction middle plane displacement, w_0

$$\kappa_x = \frac{\partial^2 w_0}{\partial x^2}, \quad \kappa_y = \frac{\partial^2 w_0}{\partial y^2}, \quad \kappa_{xy} = 2\frac{\partial^2 w_0}{\partial x \partial y} \tag{45}$$

Note that κ_{xy} represents the twist curvature of the middle plane. Fig. 3 depicts the deformation associated with a typical cross-sectional element in a thin plate.

Also, following the approach of the classical plate theory, the resultant forces and moments, instead of the stresses, are utilized in the consitutive relations. Referring to Figs. 4a and b, the force and moment resultants of the laminate are obtained by integrating the stresses of each lamina, through the laminate thickness, h

$$(N_x, N_y, N_{xy}) = \int_{-h/2}^{h/2} (\sigma_x, \sigma_y, \tau_{xy})\, \mathrm{d}z \tag{46}$$

$$(M_x, M_y, M_{xy}) = \int_{-h/2}^{h/2} (\sigma_x, \sigma_y, \tau_{xy})\, z\mathrm{d}z \tag{47}$$

Substitution of Equations 25 and 26 to 31 into Equations 43 and 44 results in the following

$$\begin{pmatrix} N_x \\ N_y \\ N_{xy} \end{pmatrix} = \begin{pmatrix} A_{11} & A_{12} & A_{16} \\ A_{12} & A_{22} & A_{26} \\ A_{16} & A_{26} & A_{66} \end{pmatrix} \begin{pmatrix} \varepsilon_x^0 \\ \varepsilon_y^0 \\ \gamma_{xy}^0 \end{pmatrix} + \begin{pmatrix} B_{11} & B_{12} & B_{16} \\ B_{12} & B_{22} & B_{26} \\ B_{16} & B_{26} & B_{66} \end{pmatrix} \begin{pmatrix} \kappa_x \\ \kappa_y \\ \kappa_{xy} \end{pmatrix} \tag{48}$$

$$\begin{pmatrix} M_x \\ M_y \\ M_{xy} \end{pmatrix} = \begin{pmatrix} B_{11} & B_{12} & B_{16} \\ B_{12} & B_{22} & B_{26} \\ B_{16} & B_{26} & B_{66} \end{pmatrix} \begin{pmatrix} \varepsilon_x^0 \\ \varepsilon_y^0 \\ \gamma_{xy}^0 \end{pmatrix} + \begin{pmatrix} D_{11} & D_{12} & D_{16} \\ D_{12} & D_{22} & D_{26} \\ D_{16} & D_{26} & D_{66} \end{pmatrix} \begin{pmatrix} \kappa_x \\ \kappa_y \\ \kappa_{xy} \end{pmatrix} \tag{49}$$

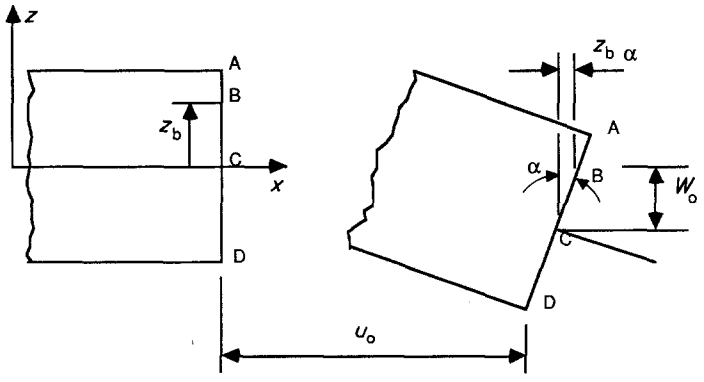

Figure 3 Deformation of a typical cross-sectional element in a thin laminated plate.

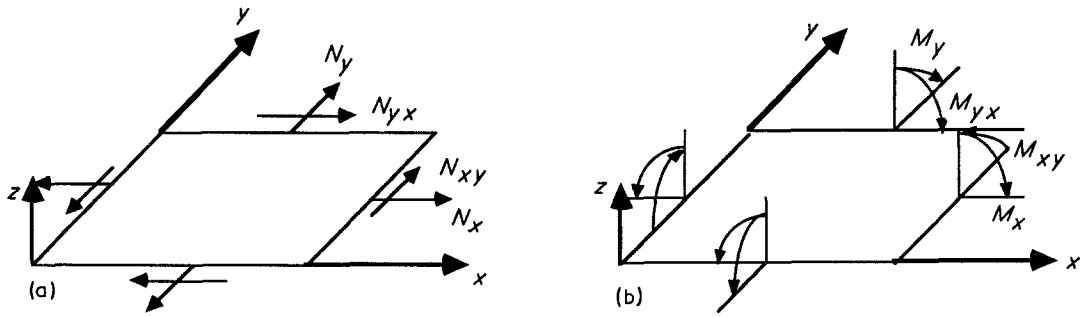

Figure 4 (a) In-plane force resultants. (b) In-plane moment resultants.

where

$$A_{ij} = \sum_{k=1}^{n} (Q_{ij})_k (z_k - z_{k-1}) \quad (50)$$

$$B_{ij} = \frac{1}{2} \sum_{k=1}^{n} (Q_{ij})_k (z_k^2 - z_{k-1}^2) \quad (51)$$

$$D_{ij} = \frac{1}{3} \sum_{k=1}^{n} (Q_{ij})_k (z_k^3 - z_{k-1}^3) \quad (52)$$

In Equations 48 to 52, the A_{ij}, B_{ij} and D_{ij} are called extensional stiffness, extension-bending coupling stiffness, and bending stiffness, respectively. The summation in Equations 50 to 52 is carried out over all the laminae: $(Q_{ij})_k$ refers to the reduced stiffness of the kth layer. In general, each stiffness matrix has nine components; these components can be simplified through a judicious selection of the orientation and location along the z-axis of the individual laminae composing the laminate [20, 21].

3. Cord/rubber composites

Cord/rubber composites for pneumatic tyres are examined in this section from the viewpoint of the mechanics of anisotropic materials. Cord/rubber composites are complex elastomeric composites composed of (a) the rubber matrix of usually quite low modulus and high extensibility, (b) the reinforcing cord of much higher modulus and lower extensibility than the matrix, and (c) the adhesive film which bonds the cord to the matrix. The combination is subjected to (a) fluctuating loads, mostly tensile but on occasion compressive, (b) temperature as high as 125° C, and (c) moisture. Obviously substantial stress develops at the cord–rubber interface. Some of the discussions presented here on the materials and mechanics aspects of pneumatic tyres are based upon the review articles of Walter [3] and Clark [26].

The construction of a tyre involves calendering sheets of rubber around an array of parallel textile cords to form a flat, essentially two-dimensional anisotropic sheet. The cords usually have substantial twist and often are made up of two or three oppositely twisted yarns. These composite sheets are then assembled into various tyre configurations. Fig. 5a shows the typical bias or angle-ply design which utilizes two or more, usually an even number, of plies laid at alternate diagonal angles to one another. Fig. 5b depicts a typical radial tyre construction consisting of a single-ply structure involving radially oriented cords while the tread area is reinforced by a belt structure of relatively small angle with respect to the tyre centre line. The radial tyre construction provides stiff longitudinal reinforcement for the tread area (and hence, is less subject to slip), and flexibility for the vertical deflection [26]. In the terminology of laminated composites, bias and radial tyres can be categorized as laminates with $[+\theta/-\theta]$ and $[+\theta/0/-\theta]$ orientations with respect to the tyre centre line.

3.1. Rubber and cord properties

For relatively small strain, rubber may be treated as a homogeneous and isotropic material. The Young's modulus, determined from the initial slope of the stress–strain curve, may be as low as 0.69 MPa (100 psi) for non-reinforced (unfilled) elastomers to as high as 689 MPa (100 000 psi) for highly vulcanized (high sulphur) compounds such as ebonite. The Young's modulus of rubber is affected by the conditions of physical testing (i.e. strain rate, temperature, cyclic

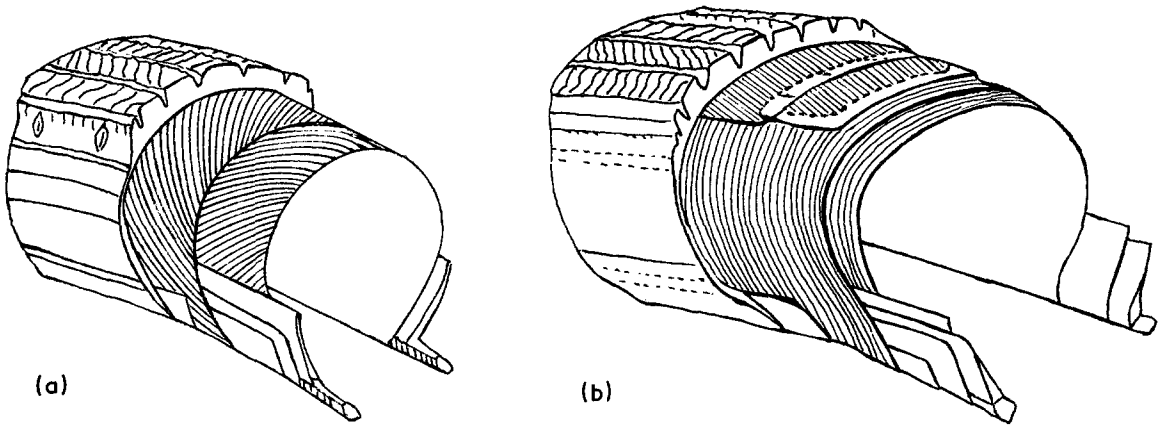

Figure 5 (a) Bias-ply tyre, after [26]. (b) Radial-ply tyre, after [26].

load history) and chemical vulcanization parameters (i.e. the compounding ingredients, state of cure) [26].

The assumption of negligible volume change of rubber, leads to $v \simeq 1/2$, $K \to \infty$, and $E \simeq 3G$. Rubbers used in calendered plies of tyres have E values of 5.51 MPa (800 psi) for textile body ply, 20.67 MPa (3000 psi) for textile tread ply and 13.78 MPa (2000 psi) for steel tread ply. The v value for these materials is 0.49.

The Young's moduli for tyre cords vary with cord constructions. The following values are for belt-ply: 109.55 GPa (15.9×10^6 psi) for steel, 24.8 GPa (3.6×10^6 psi) for Kevlar, and 11.02 GPa (1.6×10^6 psi) for rayon. The values for body-ply are: 3.96 GPa (575×10^3 psi) for polyester, and 3.45 GPa (500×10^3 psi), for nylon. Experiments have shown that textile cords can carry some load in compression, although compressive loads are believed to be the source of many textile failures and should be avoided whenever possible [25].

Twisting of the cord is needed in order to provide adequate cord fatigue life under service conditions. However, twisting of fibre into tyre cord can result in as much as a one-third decrease in tensile Young's modulus, for belt-ply cords and a one-half decrease in Young's modulus for body-ply cord. It has been predicted that the axial Young's modulus of a single twisted fibre yarn is approximately equal to $1/(1 + 4\pi^2 R^2 T^2)$ of that of the untwisted yarn. Here R and T denote yarn radius and the twist (number of turns per unit length), respectively [27]. The twisted and multi-plied cords should be considered as transversely isotropic, although they are commonly approximated as isotropic. Textile cords normally show substantial non-linearity in their stress–strain behaviour. However, because the rubber behaviour is relatively elastic in the small strain range, and the cords in a laminate are often aligned at an angle to the load direction, the composite acts more like a linearly elastic solid than the cord itself [26]. Fig. 6 shows the stress–strain curve of a tubular specimen using rayon yarn in a rubber matrix [26]. The fibres in this specimen are in angle-ply arrangement. According to Clark, most pneumatic tyres do not operate with strain much in excess of 10%.

3.2. Unidirectional cord/rubber composite

Adkins and Rivlin [28] first presented the analysis of a thin sheet containing a double layer of cords subjected to a pure homogeneous strain. The matrix material is assumed to be isotropic and incompressible and the cords are thin, flexible and inextensible.

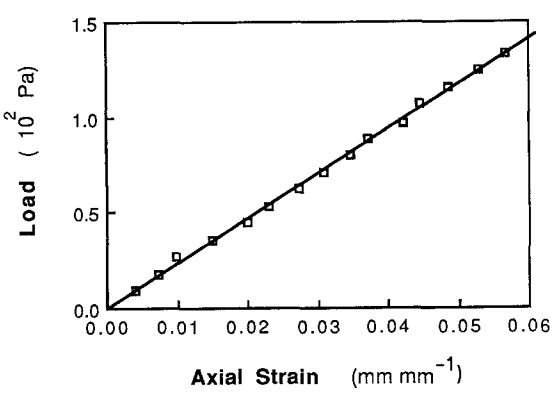

Figure 6 Load–strain curve of a cylindrical tube with rayon yarns in a rubber matrix, after [26].

The linear elastic behaviour of a unidirectional cord/rubber composite can be easily deduced from the basic equations given in Section 2.1. By assuming that $E_f \gg E_m$, and $v_m \simeq 0.5$, Akasaka [29] obtained the following approximations

$$E_1 \simeq E_f V_f \gg E_2 \tag{53}$$

$$E_2 \simeq \frac{4}{3}\frac{E_m}{V_m} \tag{54}$$

$$v_{21} \simeq 0, \tag{55}$$

$$G_{12} \simeq \frac{G_m}{V_m} \simeq \frac{E_2}{4} \tag{56}$$

Akasaka [29] has noted that the expression of $G_{12} \simeq E_2/4$ is independent of cord volume fraction and has good predicability as compared to existing formulae and experimental results [30, 31].

It should also be noted that using the assumptions of $E_f \gg E_m$, and $v_m \simeq 0.5$, Equations 2 and 4 yields the following results:

$$E_2 = \frac{(1 + 1.3V_f)E_m}{(1 + 0.5V_f)V_m} \tag{57}$$

$$G_{12} = \frac{G_m}{V_m}(1 + V_f) \tag{58}$$

and G_{12} is not independent of cord volume fraction. Also, if the unidirectional composite is approximated as cord and rubber components loaded in series or in parallel [22], predictions different from Equations 53 to 56 are obtained

$$E_2 \simeq \frac{E_m}{V_m} \tag{59}$$

$$G_{12} \simeq \frac{G_m}{V_m} \simeq \frac{E_2}{3} \tag{60}$$

Based upon Equations 53 to 60, the variation of lamina transformed reduced stiffness with cord off-axis angle, θ, follows from Equations 26 to 31 and can be approximated as [32]

$$Q_{11} \simeq E_2 + E_1 \cos^4\theta \tag{61}$$

$$Q_{22} \simeq E_2 + E_1 \sin^4\theta \tag{62}$$

$$Q_{66} \simeq E_2/4 + E_1 \sin^2\theta \cos^2\theta \tag{63}$$

$$Q_{12} \simeq E_2/2 + E_1 \sin^2\theta \cos^2\theta \tag{64}$$

$$Q_{16} \simeq E_1 \sin\theta \cos^3\theta \tag{65}$$

$$Q_{26} \simeq E_1 \sin^3\theta \cos\theta \tag{66}$$

When a unidirectional cord/rubber sheet is subjected to simple tension, an interesting deformation behaviour occurs, which is not observed in rigid composites [29]. This can be elucidated by using Equation 32 for the relation between γ_{xy} and the applied σ_x as well as the approximations of Equations 53 to 60

$$\gamma_{xy} = S_{16}\sigma_x \simeq \frac{-2 \sin\theta \cos^3\theta}{E_2}(2\text{-}\tan^2\theta)\sigma_x \tag{67}$$

Thus, the stretching–shear coupling vanishes at $\theta \simeq 54.7°$, and $\gamma_{xy} < 0$ for $\theta < 54.7°$ and $\gamma_{xy} > 0$ for $\theta > 54.7°$. The positive θ direction is defined in Fig. 5.

3.3. Laminated cord/rubber composites

The simple case of laminated composite in the form of a $[+\theta/-\theta]$ angle-ply was first examined by Clark [32]. Obviously, from Equations 48 and 50 the A_{ij} matrix components (divided by the ply thickness h) can be expressed as

$$2A_{ij}/h = \begin{pmatrix} Q_{11}(\theta) + Q_{11}(-\theta) & Q_{12}(\theta) + Q_{12}(-\theta) & 0 \\ 0 & Q_{22}(\theta) + Q_{22}(-\theta) & 0 \\ 0 & 0 & Q_{66}(\theta) + Q_{66}(-\theta) \end{pmatrix} \quad (68)$$

The A_{ij} matrix (divided by the ply thickness) of Equation 68 and the Q_{ij} matrix of Equation 16 are of the same general form. Thus, the engineering elastic constants, referring to the x–y coordinate system, for the angle-ply laminated composite can be deduced in the same manner as those given by Equations 21 to 24. Using the results of Equations 53 to 56 and 61 to 66, the following expressions of engineering elastic constants are obtained.

$$E_x = E_f V_f \cos^4\theta + 4G_m/(1 - V_f) - [E_f V_f \sin^2\theta \cos^2\theta + 2G_m/(1 - V_f)]^2/[E_f V_f \sin^4\theta + 4G_m/(1 - V_f)] \quad (69)$$

$$E_y = E_x(\pi/2 - \theta) \quad (70)$$

$$G_{xy} = E_f V_f \sin^2\theta \cos^2\theta + G_m/(1 - V_f) \quad (71)$$

$$\nu_{xy} = [E_f V_f \sin^2\theta \cos^2\theta + 2G_m/(1 - V_f)]/[E_f V_f \sin^4\theta + 4G_m/(1 - V_f)] \quad (72)$$

$$\nu_{yx} = \nu_{xy}(\pi/2 - \theta) \quad (73)$$

The approach for obtaining Equations 69 to 73 based upon the assumptions of $\pm\theta$ cord angles and especially orthotropic symmetry is known as the modified netting analysis. Walter [3] obtained expressions similar to Equations 69 to 73, with slight variations in the approximation for G_{12}.

The classical netting analysis which assumes inextensible cords ($E_f \to \infty$) simplifies Equations 69 to 73

$$E_x = 4G_m(1 - V_f)(\cot^4\theta - \cot^2\theta + 1) \quad (74)$$

$$E_y = E_x(\pi/2 - \theta) \quad (75)$$

$$G_{xy} = E_f V_f \sin^2\theta \cos^2\theta + G_m(1 - V_f) \quad (76)$$

$$\nu_{xy} = \cot^2\theta \quad (77)$$

$$\nu_{yx} = \tan^2\theta \quad (78)$$

Figs 7 to 9 show the results of analytical predictions based upon Equation 68 for E_x, G_{xy}, and ν_{xy}, respectively, as functions of the off-axis angle, θ. These results coincide very well with the experimental data, also reported by Clark [32] and based upon $E_1 = 1440$ MPa and $E_2 = 6.9$ MPa. It is evident that Poisson's ratios well in excess of one-half exist in cord-rubber composites.

Walter [3] compared the variations of E_x, G_{xy} and ν_{xy} with cord orientation for 1- and 4-ply laminates. It is noted that the maximum values of ν_{xy} of a nylon–rubber system are attained for $\theta \approx 20°$ in both 1-ply ($\nu_{xy} \approx 1$) and 4-ply ($\nu_{xy} = 4$) constructions. The significant Poisson mismatch for cord angle θ between 40° and 5° indicates a source of interlaminar stress between the body and belt of a radial tyre.

Because of the incompressibility of the rubber matrix and the relatively small volume change associated with the cord materials, due to its high stiffness, it can be assumed that the cord/rubber composite is incompressible. Thus, for small strain, $\varepsilon_x + \varepsilon_y + \varepsilon_z = 0$, and

$$\nu_{xz} = -\varepsilon_z/\varepsilon_x = 1 + \varepsilon_y/\varepsilon_x = 1 - \nu_{xy} \quad (79)$$

Fig. 10 indicates the analytical results of Equation 79 and experimental data of ν_{xz} as a function of θ [28] for $E_1 = 294$ MPa and $E_2 = 6.6$ MPa. One of the solid lines is based upon Equation 72 and the simplifying expressions of Equations 53 to 56 namely

$$\nu_{xy} = \frac{E_1 \sin^2\theta \cos^2\theta + E_2/2}{E_1 \sin^4\theta + E_2} \quad (80)$$

The other solid line is based upon Equation 77. It is interesting to note that for a range of θ values, ν_{xz} is negative; the laminate becomes thicker under axial load.

The lamination theory introduced in this review does not take into account the interlaminar stresses σ_z, τ_{zx} and τ_{zy}. These stresses and their corresponding strains do exist in appreciable magnitude which promote a reduction in the apparent stiffness of cord–rubber laminates. As a result, the composite becomes more flexible and exhibits lower natural frequencies of vibration and static buckling loads [3].

The analytical treatment of interlaminar stresses has been discussed by Vinson and Chou [21], Walter [3] reviewed the work of Kelsey, who considered a two-ply $\pm\theta$ cord–rubber laminate, simulating the behaviour of the belt in a radial tyre. Assuming the belt of finite width in the y direction is loaded in the x direction, γ_{yz} vanishes due to symmetry and ε_z is

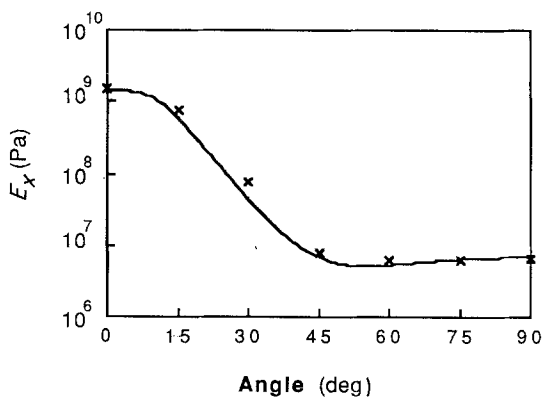

Figure 7 Young's modulus E_x plotted against cord angle θ for a two-ply laminate [33]. (——) Equation 69, (x) experimental data.

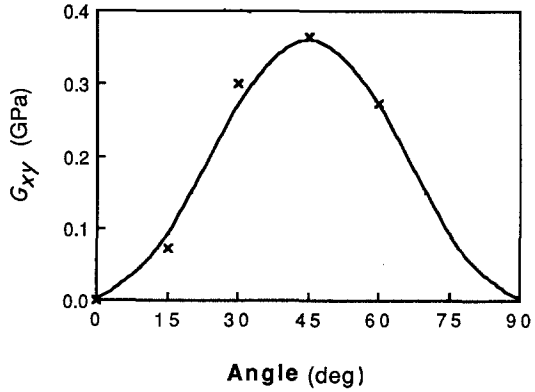

Figure 8 Shear modulus G_{xy} plotted against cord angle θ for a two-ply laminate [33]. (——) Equation 71, (x) experimental data.

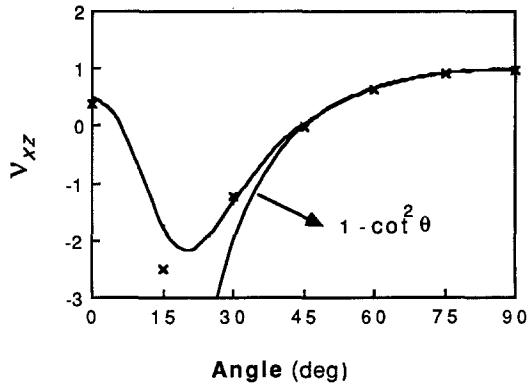

Figure 10 Poisson's ratio ν_{xz} plotted against cord angle θ for a two-ply laminate [29]. Based on Equations 77 and 81, (x) experimental data.

assumed to be negligibly small. γ_{xz} is maximum at the free edge of the belt and can be approximated, for the case of inextensible cords ($E_f \rightarrow \infty$), by the simple expression

$$\gamma_{xz} = \varepsilon_x(2 \cot^2\theta - 1) \quad (81)$$

Equation 81 indicates that γ_{xz} vanishes when the two plies are oriented at $\theta = \pm \cot^{-1} 1/2 = \pm 54.7°$. The magnitude of γ_{xz} decays exponentially away from the free edge and vanishes along the belt centreline ($y = 0$); also it is of opposite sign at each belt edge. It is interesting to note that $\theta = 54.7°$ is also the angle for which the normal stress and shear strain are uncoupled and each off-axis ply behaves as especially orthotropic.

Interlaminar shear strains have been observed by inserting straight pins normal to the ply surface in a cord–rubber belt system and observing its rotation under extensional load [34] or by scribing a straight line on the edge of the specimen and monitoring the rotation of line under load. Fig. 11 shows the interlaminar shear strain measured by X-ray technique for a two-ply polyester–rubber as a function of cord angle θ [35]. The solid line is based upon the predictions of Equation 82. The importance of interlaminar shear decreases as the number of ply increases.

Walter [3] has presented values of the 18 elastic constants of A_{ij}, B_{ij} and D_{ij} for bias, belted-bias and radial ply constructions; the material combinations of nylon and raylon body plies with steel, PVA and rayon belt plies are included.

For the case of a specially orthotropic laminate (A_{16}, A_{26}, D_{16}, D_{26}, $B_{ij} = 0$) with respect to the x–y axes, the out-of-plane flexural rigidities are

$$(EI)_x = A_{11}h^2/12 = E_1h^3/12(1 - \nu_{xy}\nu_{yx}) \quad (82)$$

$$(EI)_y = A_{22}h^2/12 = E_2h^3/12(1 - \nu_{yx}\nu_{xy}) \quad (83)$$

where h denotes ply thickness.

3.4. Remarks on cord loads in tyres

According to Clark [26] the key to good tyre design is long fatigue life. The loads on typical textile cords in pneumatic tyres are extremely complex and the sources of loads can be identified as follows: (a) inflation load, (b) vertical load, (c) steering forces, (d) road irregularities, (e) camber, (f) speed, and (g) torque.

The tensile cord load due to inflation pressure can be predicted with some certainty by considering the axisymmetric nature of inflation and approximating the tyre geometry as a thin toroidal shell. However, this task is complicated by the fact that the tyre does not maintain a constant geometry during inflation. Furthermore, the membrane forces obtained from the thin shell analysis may not adequately represent the force distributions in the bead and tread regions. Fig. 12 shows schematically the cross-section of a pneumatic tyre and the designation of the locations [26].

The measurement of cord loads is important to the analysis and design of tyres. Various techniques have been employed; these include the use of grid or elongation marks for outer plies, X-ray photography relying on metal markers for inner plies, and resistance foil

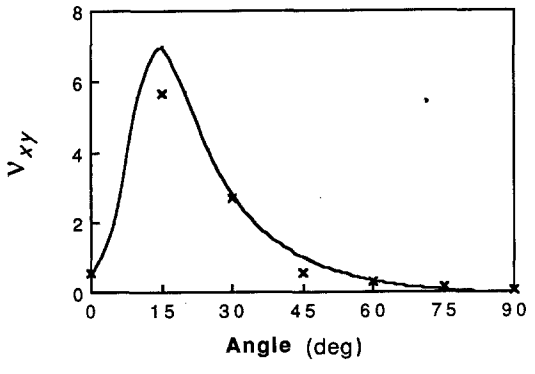

Figure 9 Poisson's ratio ν_{xy} plotted against cord angle θ for a two-ply laminate [33]. (——) Equation 72, (x) experimental data.

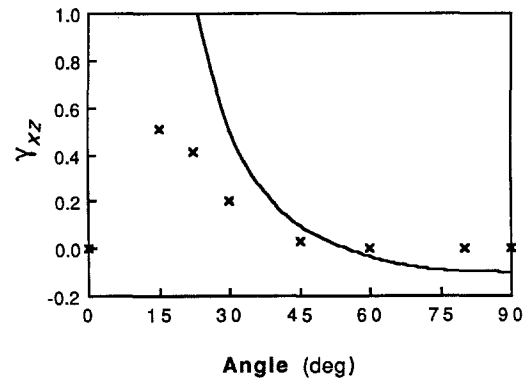

Figure 11 Interlaminar shear strain γ_{xz} plotted against cord angle θ for a two-ply polyester rubber. (——) Equation 82, (x) experimental data [35].

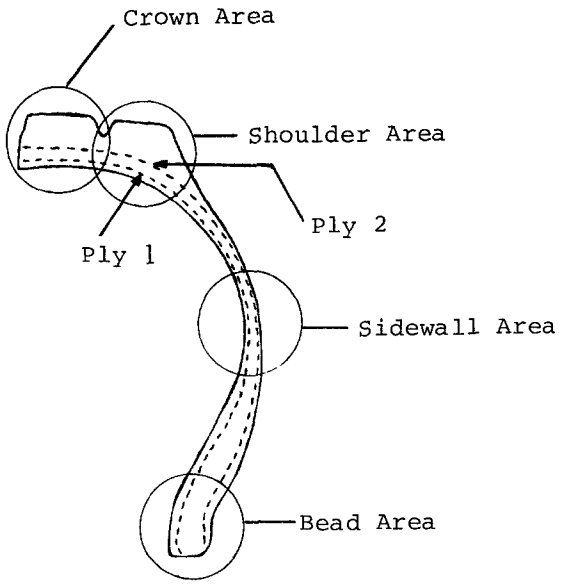

Figure 12 Location description in a cord/rubber pneumatic tyre, after [26].

strain gauges embedded in the tyre for direct cord load measurement in a tyre under operating conditions. The force transducers using resistance foil strain gauges are much smaller than the clip gauges, the rubber–wire gauges, or the liquid metal gauges. Details of these measurement techniques can be found in [36–39].

The measurements of tyre cord loads have indicated that the loads induced by normal direct inflation account for about 10 to 15% of cord strength. Another simple type of cord load is induced due to the load carried by the tyre. The cord load at a given location can fluctuate fairly widely as the tyre rolls. These fluctuations occur, for instance, in the crown region of a bias-ply tyre and the load is lessened as the tyre cord rolls through the tyre contact patch. The typical cord load cycle varies with the locations on the tyre, i.e. crown, sidewall or shoulder region. Steering induces additional loads. Relatively small amounts of steer could induce very large increases in the cord loads. Fig. 13 shows the basic characteristics of cord load fluctuation in a rolling tyre [26]. It should be noted that compressive cord loads are possible. The characteristics of other cord loads due to road irregularities, speed and torque are even more difficult to quantify in a systematic manner.

The measurement of tyre cord loads provides the basis of analysis of the response of cord/rubber composites to the specified boundary conditions. The net

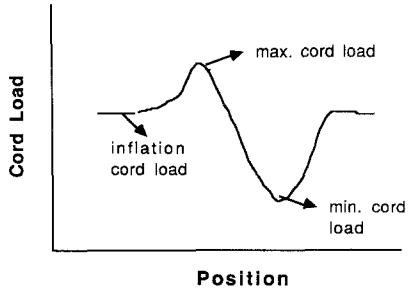

Figure 13 Basic characteristics of cord load fluctuation in a rolling tyre, after [26].

theory, which only takes into account the deformation of the cord and neglects completely the contribution of the matrix rubber, was adopted in the earlier research of bias constructions. The uncertainty of the orientation of the cord in the net structure at different stress levels of inflation has limited the applicability of this theory.

The theory of laminated composite has undoubtedly provided an efficient means of analysis of cord/rubber composites. It is understood that the theory has its limitations for the following reasons.

1. Textile cord strains of several per cent could develop at some locations in the tyre; even larger and non-linear strains could develop in the rubber.
2. Interlaminar deformations are not taken into account in the theory, assuming plane stress condition.
3. Cord/rubber composites usually exhibit bimodulus behaviour [40, 41].
4. The viscoelastic behaviour is assumed to be small and often neglected in the analysis.
5. Perfect cord/rubber interfacial bonds are assumed.
6. The membrane forces in the bead and tread regions may be very complex.
7. Fatigue and hygrothermal loadings may also complicate the problem.

However, in spite of its limitations, the lamination theory has been applied with some success for investigating a number of tyre mechanics problems including stress analysis, obstacle enveloping, treadwear, vibration and ply steer [3]. It is thus an efficient tool based upon linearly elastic, homogeneous and anisotropic material properties for the representation of non-linear viscoelastic, heterogeneous calendered plies of cord/rubber tyre composites [3]. The large non-linear deformation of flexible composites is treated in Section 5.

4. Coated fabrics

Coated fabrics used in a load-bearing environment, for instance, those for air- or cable-supported building structures, tents, and inflated structures such as escape slides, must exhibit specific mechanical properties. Some of the general requirements include retaining flexibility over a wide temperature range, sufficient tensile and tear strength, low air permeability, and sufficient dimensional stability [14].

It has been recognized that coated fabrics generally exhibit nonlinear stress–strain behaviour due to the straightening of the crimped yarns under uniaxial or biaxial tension. As noted by Akasaka [29], the microscopic deformation behaviour of the woven yarns embedded in the matrix and subjected to membrane loading is very complex. Thus, modelling of the strength behaviour of these materials requires reasonably precise knowledge of the deformation of the yarns as a function of load configuration and magnitude.

The linear elastic properties of laminates composed of coated fabrics can be readily derived based upon the lamination theory of Section 2. Akasaka and Yoshida [16] presented explicit expressions for elastic moduli of laminates of coated fabrics; the analytical predictions were compared with experimental data of laminate of canvas.

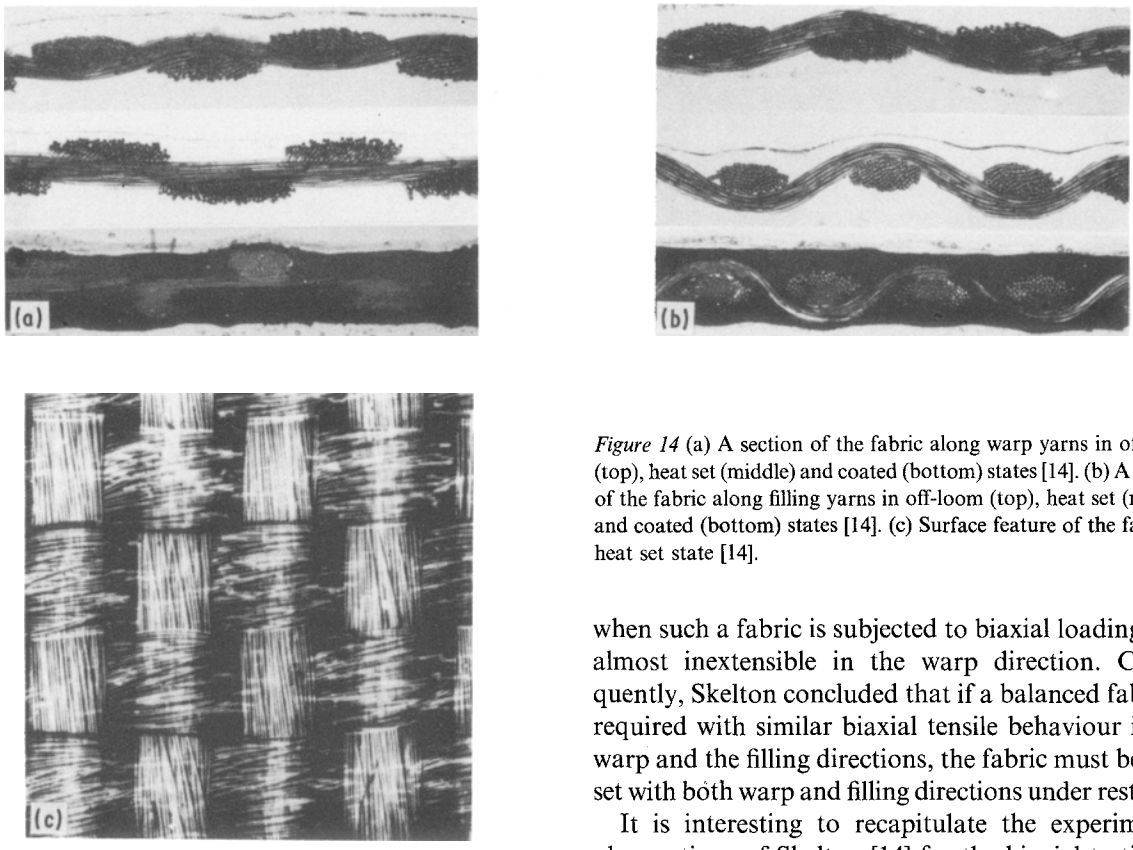

Figure 14 (a) A section of the fabric along warp yarns in off-loom (top), heat set (middle) and coated (bottom) states [14]. (b) A section of the fabric along filling yarns in off-loom (top), heat set (middle) and coated (bottom) states [14]. (c) Surface feature of the fabric in heat set state [14].

Skelton [14], among others, reported the biaxial stress–strain behaviour of coated orthogonal fabrics. It is concluded that the stress–strain response at various stages of manufacture of coated fabrics is dependent mainly on the crimp in the two sets of yarns. The balance of crimp is determined by the restraints imposed on the fabric during the heat setting process, which precedes the coating operation. If the fabric is set under tension in the warp direction, the warp yarns tend to become straight and the yarns in the filling direction become highly crimped. Thus, when such a fabric is subjected to biaxial loading, it is almost inextensible in the warp direction. Consequently, Skelton concluded that if a balanced fabric is required with similar biaxial tensile behaviour in the warp and the filling directions, the fabric must be heat set with both warp and filling directions under restraint.

It is interesting to recapitulate the experimental observations of Skelton [14] for the biaxial testing of coated fabrics. Figs 14a and b show, respectively, the section views of a plain weave fabric based upon high tenacity polyester. Because the fabric is set under tension along the warp direction during heat setting, the warp crimp is minimum and the filling crimp is relatively high. Three stages, i.e. off-loom, heat set and coated state, are demonstrated. Fig. 14c shows the surface features of the fabric in heat set state.

Fig. 15 shows the biaxial load–elongation curves for this fabric with load ratio (warp/filling) = 1 : 2. The biaxial behaviour can be understood by bearing in

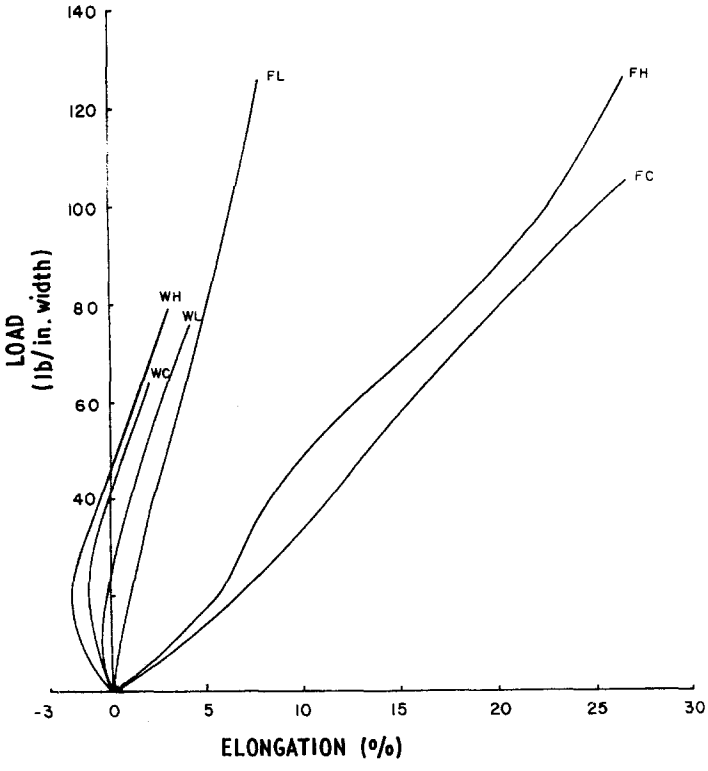

Figure 15 Biaxial load–elongation curves for a fabric; load ratio (warp/fill) = 1 : 2. WL = warp direction, loom state, FL = filling direction, loom state, WH = warp direction, heat set, FH = filling direction, heat set, WC = warp direction, coated, FC = filling direction, coated [14].

mind that in the heat set state the crimp is unbalanced; the warp yarns are essentially straight and the filling yarns are highly crimped. Thus, according to Skelton, the extension of the highly crimped direction of the filling yarns, brings about an increase in crimp and reduction in width in the warp direction, in spite of the applied load in that direction. Consequently, the load–elongation curve shows negative elongation in the warp direction at low load level.

The elastic and inelastic response of coated fabrics has been studied by Stubbs and Thomas [15] using a space truss model. The model is capable to account for arbitrary loading sequences.

5. Non-linear elastic behaviour – incremental analysis

The flexible composites discussed in this section are also composed of continuous fibres in an elastomeric matrix. Because of the low shear modulus of the matrix and the highly anisotropic nature ($E_1 \gg E_2$) of the composites, their effective elastic properties are very sensitive to the fibre orientation. The geometric non-linearity of the flexible composite is mainly caused by the reorientation of fibres. The material non-linearity is also pronounced in elastomeric composites under large deformation.

The finite deformation and non-linear elastic behaviour of flexible composites are examined using two approaches. In this section, the work of Chou and Takahashi [1] is recapitulated. The non-linear constitutive relation is predicted based upon a step-wise incremental analysis and the classical lamination theory. Both fibre geometric non-linearity and matrix material non-linearity have been taken into account. Because of the superposition of the infinitesimal solutions from lamination theory, the limitation of this approach is obvious. However, being a well-established analytical technique in the composites field, the lamination theory does provide a convenient tool for discerning the basic characteristics of flexible composites.

In the second approach presented in Section 6, a mathematical model of the constitutive relation is established based upon the Eulerian description of the deformation to account for the material non-linearity, including stretching–shear coupling.

Comparisons are made between the analytical predictions of these two approaches and experimental data for tyre cord/rubber and carbon and Kevlar/silicone–elastomer flexible composite laminae. Because composites with fibres in wavy form have been used as a model system, the geometric aspects of curved fibres are presented first.

5.1. Geometry of curved fibres

To demonstrate the effect of fibre extensibility from geometric design, a flexible composite composed of continuous fibres with sinusoidal waviness in a ductile matrix is studied. Perfect bonding between the fibres and matrix is assumed. The geometric relations between the wavelength (λ), amplitude (a), and fibre length (s) of a sinusoidal-shaped fibre are identified first. Then, two types of fibre arrangement are considered: the iso-phase model, and the random-phase model. The fibres are assumed to maintain the sinusoidal shape of which the geometric parameters λ, a and s vary with the increase of the applied load.

The spatial position of a typical fibre in the xyz coordinates is given by

$$y = a \sin \frac{2\pi x}{\lambda} \tag{84}$$

where the parameters a and λ of the curved fibre are shown in Fig. 16. The angle (θ) between the tangent to the fibre and the x-axis is a function of x.

$$\tan \theta = \frac{dy}{dx} = \frac{2\pi a}{\lambda} \cos \frac{2\pi x}{\lambda} \tag{85}$$

The length of fibre, ds, between x and $x + dx$ is

$$\begin{aligned} ds &= (dx^2 + dy^2)^{1/2} \\ &= dx \left[1 + c \cos^2 \left(\frac{2\pi x}{\lambda}\right)\right]^{1/2} \end{aligned} \tag{86}$$

where $c = (2\pi a/\lambda)^2$. Obviously, the maximum value of $\tan \theta$ occurs at

$$|\theta_{max}| = \tan^{-1} \left(\frac{2\pi a}{\lambda}\right) \tag{87}$$

The fibre length, s, between $x = 0$ and λ is given by

$$\begin{aligned} s &= \int ds \\ &= \frac{\lambda}{2\pi} \int_0^{2\pi} (1 + c \cos^2 \beta^{1/2}\ d\beta) \end{aligned} \tag{88}$$

By the use of elliptic integral of the second kind

$$\begin{aligned} s = {} & \lambda(1 + c)^{1/2} \\ & \times \left(1 - \frac{1}{2^2} k^2 - \frac{1^2 3}{2^2 4^2} k^4 - \frac{1^2 3^2 5}{2^2 4^2 6^2} k^6 - \cdots\right) \end{aligned} \tag{89}$$

where $k^2 = c/(1 + c)$. Equation 89 can be written as

$$\begin{aligned} \frac{s}{\lambda} = {} & \frac{1}{(1 - k^2)^{1/2}} \left(1 - 2\left(\frac{k^2}{8}\right) - 3\left(\frac{k^2}{8}\right)^2 \right. \\ & \left. - 10\left(\frac{k^2}{8}\right)^3 - \frac{175}{4}\left(\frac{k^2}{8}\right)^4 - \frac{441}{2}\left(\frac{k^2}{8}\right)^5 - \cdots\right) \end{aligned} \tag{90}$$

By the use of Taylor expansion, we have

$$\begin{aligned} \frac{s}{\lambda} = {} & 1 + 2\left(\frac{k^2}{8}\right) + 13\left(\frac{k^2}{8}\right)^2 + 90\left(\frac{k^2}{8}\right)^3 \\ & + 644\left(\frac{k^2}{8}\right)^4 + 4708.5\left(\frac{k^2}{8}\right)^5 + \cdots \end{aligned} \tag{91}$$

In the following analysis, terms up to $(k^2/8)^5$ are taken into account in Equation 91 and the range of a/λ is limited to below 1/5. The relationship between a/λ and s/λ is shown in Fig. 16 where θ_{max} is the maximum angle between the fibre and the x-axis. For example, for $\theta_{max} = 20°$, $a/\lambda = 0.058$ and $s/\lambda = 1.032$. The curved fibre composite with $s/\lambda = 0.10$ can be extended up to 9.23% of its original length only by the straightening of the fibre, if the matrix stiffness is negligible.

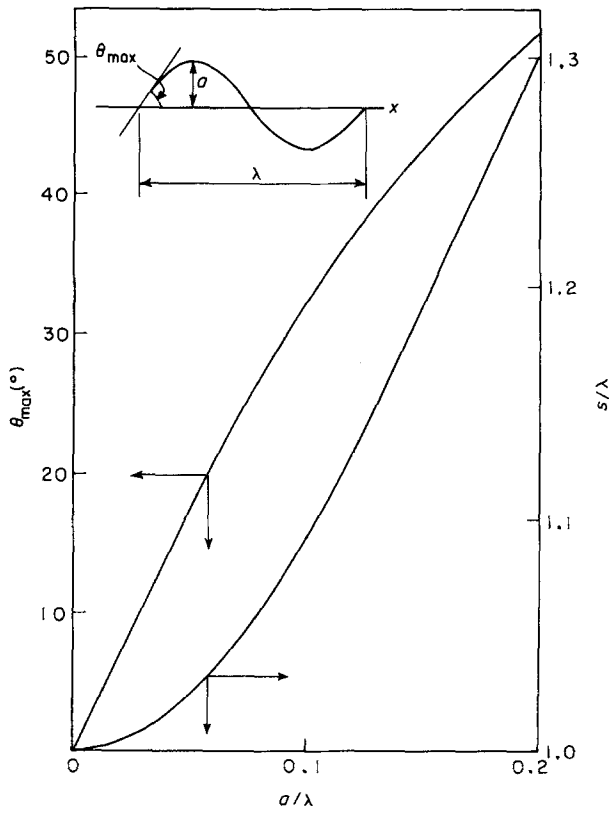

Figure 16 Geometrical relationships between a/λ, s/λ and θ_{max}, where θ_{max} is the maximum angle between the fibre and x-axis [1].

Two kinds of arrangements of the curved fibres in the composite are considered, the iso-phase model and random-phase model. The iso-phase model is defined by Fig. 17, where all the fibres are in the same phase in the x-direction. The distance between the fibres in the y-direction is assumed to be constant. In the random phase model (Fig. 18), the axial locations of sinusoidal shaped fibres do not assume any regular pattern.

5.2. Axial tensile behaviour

The non-linear tensile stress–strain behaviour of flexible composites containing curved fibres is investigated according to the iso-phase and random-phase models. The lamination theory developed in Section 2 is used for this purpose. The applied load is parallel to the axes of the sinusoidally-shaped fibres.

5.2.1. Iso-phase model

The linear elastic stress–strain relations are derived first. Consider Fig. 17; each volume element between

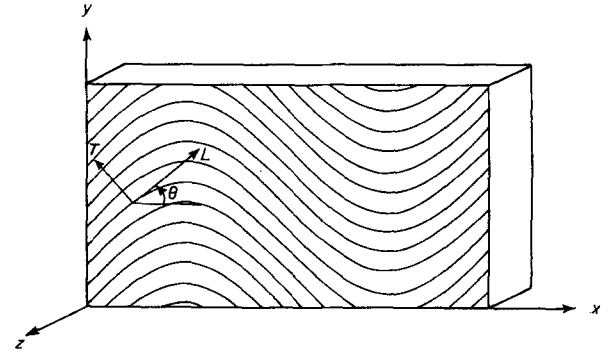

Figure 17 Iso-phase model [1].

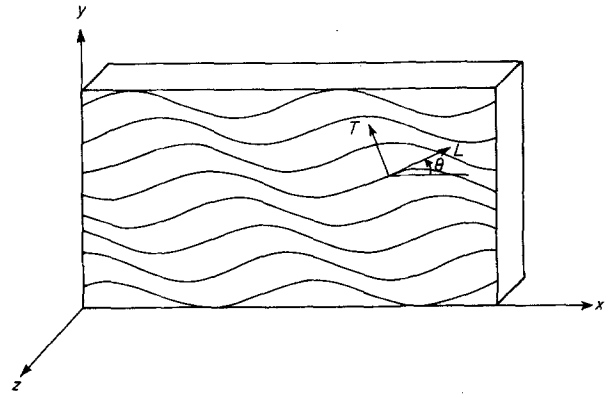

Figure 18 Random-phase model [1].

x and $x + dx$ is approximated by a unidirectional straight fibre composite, in which fibres are inclined at an angle θ to the x-axis, as defined by Equation 85. The transformation of coordinates between the composite reference axes (xyz) and the fibre local axes (LTz) is given by:

$$\begin{pmatrix} L \\ T \\ z \end{pmatrix} = \begin{pmatrix} \cos\theta & \sin\theta & 0 \\ -\sin\theta & \cos\theta & 0 \\ 0 & 0 & 1 \end{pmatrix} \begin{pmatrix} x \\ y \\ z \end{pmatrix} \quad (92)$$

The positive direction of θ is defined in Fig. 17. The strain–stress relations for the unidirectional straight fibre composite, referring to the LT system, are given by Equations 12 to 15. Under the uniaxial tension, σ_x, Equations 32 gives

$$\varepsilon_x = \boldsymbol{S}_{11}\sigma_x \quad (93)$$

$$\varepsilon_y = \boldsymbol{S}_{12}\sigma_x \quad (94)$$

$$\gamma_{xy} = \boldsymbol{S}_{16}\sigma_x \quad (95)$$

It is interesting to note the stretching–shear coupling represented by $\boldsymbol{S}_{16}$. Fig. 19 shows schematically the γ_{xy} induced by an applied stress σ_x for glass/polybutylene terephthalate (PBT) composite.

The average tensile strain of the iso-phase composite, ε_x^*, is

$$\varepsilon_x^* = \frac{1}{\lambda}\int_0^s \varepsilon_x \, dx \quad (96)$$

From Equations 85 and 93 to 95 we obtain

$$\varepsilon_x^* = \left(\frac{1 + (c/2)}{(1 + c)^{3/2}} S_{11} - \left(\frac{1 + (3/2)c}{(1 + c)^{3/2}} - 1\right) S_{22} + \frac{c/2}{(1 + c)^{3/2}} (2S_{12} + S_{66})\right) \sigma_x \quad (97)$$

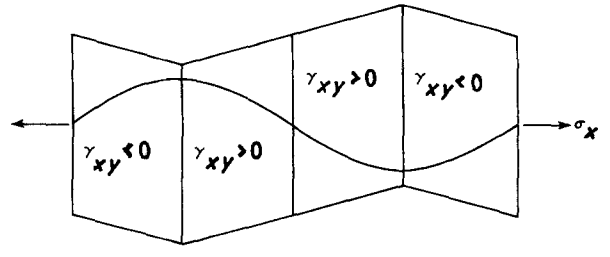

Figure 19 Schematic illustration of the deformed shape of the iso-phase model under uniaxial tension σ_x, for a glass/PBT composite [1].

The effective Young's modulus of the iso-phase model in the x-direction is given by

$$E_x^* = (1 + c)^{3/2} \Big/ \left\{ \left(1 + \frac{c}{2}\right) S_{11} - [1 + \tfrac{3}{2}c - (1 + c)^{3/2}] S_{22} + \frac{c}{2}(2S_{12} + S_{66}) \right\} \quad (98)$$

In a small volume element between x and $x + \mathrm{d}x$, the tensile strain of the fibre along its axial direction is expressed by

$$\varepsilon_L = \cos^2\theta\, \varepsilon_x + \sin^2\theta\, \varepsilon_y + \sin\theta \cos\theta\, \gamma_{xy} \quad (99)$$

Substituting Equations 93 to 95 into Equation 99, and averaging over S, we have:

$$\varepsilon_L^* = \frac{1}{s}\int_0^s \varepsilon_L \,\mathrm{d}s = [(S_{11} - S_{12})F(k) + S_{12}]\sigma_x \quad (100)$$

where

$$F(k) = 1 - \frac{1}{2}k^2 - \frac{3}{16}k^4 - \frac{3}{32}k^6 - \frac{111}{2048}k^8 - \frac{141}{4096}k^{10} \quad (101)$$

Here, the relations between s, x and λ, Equations 85 to 90, and the elliptic integral are used in the derivations.

5.2.2. Random phase model

In the case of the iso-phase model, the stretching–shear coupling constants S_{16} and S_{26} do not vanish. This coupling effect could be eliminated through the random positioning of curved fibres along the x-direction.

$$y = a \sin [2\pi(x - d)/\lambda] \quad (102)$$

where d is the translation of the fibre in the x-direction. A random distribution of d ($0 \leqslant d \leqslant \lambda$) is assumed in this model. That is, in each infinitesimal section ($x \sim x + \mathrm{d}x$), the fibres with any arbitrary orientation angle exist with the same probability. Therefore, it is assumed that ε_x is uniform throughout the sample under uniaxial tension. The stress in a fibre segment depends on its orientation, θ

$$-\frac{2\pi a}{\lambda} \leqslant \tan\theta \leqslant \frac{2\pi a}{\lambda} \quad (103)$$

By these assumptions, the classical laminate theory can again be applied.

The stress–strain relations of a unidirectional lamina consisting of straight fibres are given by Equation 16 with the reduced stiffness Q_{ij} given by Equations 17 to 20. The transformed stress–strain relations of an off-axis lamina, referring to the xy coordinate system are given by Equations 25 to 31. The small element of the random-phase composite situated between the sections at x and $x + \mathrm{d}x$ is treated as a laminate with different orientations. The fibres with the orientation angle θ which lies in the range defined by

$$\frac{2\pi a}{\lambda}\cos\frac{2\pi x}{\lambda} \leqslant \tan\theta \leqslant \frac{2\pi a}{\lambda}\cos\frac{2\pi(x + \mathrm{d}x)}{\lambda} \quad (104)$$

have the probability $\mathrm{d}x/\lambda$.

Therefore, the stress–strain relation of the laminate can be rewritten as

$$\begin{pmatrix}\sigma_x\\ \sigma_y\\ \tau_{xy}\end{pmatrix} = \begin{pmatrix}C_{11}^* & C_{12}^* & C_{16}^*\\ C_{12}^* & C_{22}^* & C_{26}^*\\ C_{16}^* & C_{26}^* & C_{66}^*\end{pmatrix}\begin{pmatrix}\varepsilon_x\\ \varepsilon_y\\ \gamma_{xy}\end{pmatrix} \quad (105)$$

where

$$C_{mn}^* = \frac{1}{\lambda}\int_0^\lambda Q_{mn}(\theta)\,\mathrm{d}x \quad (106)$$

The average stiffness constants of Equation 106 are

$$C_{11}^* = \frac{1}{(1 + c)^{3/2}}\left\{Q_{11}\left(1 + \frac{c}{2}\right) + (Q_{12} + 2Q_{66})c + Q_{22}[(1 + c)^{3/2} - (1 + \tfrac{3}{2}c)]\right\} \quad (107)$$

$$C_{22}^* = \frac{1}{(1 + c)^{3/2}}\left\{Q_{11}[(1 + c)^{3/2} - (1 + \tfrac{3}{2}c)] + (Q_{12} + 2Q_{66})c + Q_{22}\left(1 + \frac{c}{2}\right)\right\} \quad (108)$$

$$C_{12}^* = \frac{1}{(1 + c)^{3/2}}\left\{(Q_{11} + Q_{22} - 4Q_{66})\frac{c}{2} + Q_{12}[(1 + c)^{3/2} - c]\right\} \quad (109)$$

$$C_{66}^* = \frac{1}{(1 + c)^{3/2}}\left\{(Q_{11} + Q_{22} - 2Q_{12} - 2Q_{66})\frac{c}{2} + Q_{66}[(1 + c)^{3/2} - c]\right\} \quad (110)$$

$$C_{16}^* = C_{26}^* = 0 \quad (111)$$

Inversion of Equation 105 leads to

$$\begin{pmatrix}\varepsilon_x\\ \varepsilon_y\\ \gamma_{xy}\end{pmatrix} = \begin{pmatrix}S_{11}^* & S_{12}^* & 0\\ S_{12}^* & S_{22}^* & 0\\ 0 & 0 & S_{66}^*\end{pmatrix}\begin{pmatrix}\sigma_x\\ \sigma_y\\ \tau_{xy}\end{pmatrix} \quad (112)$$

where

$$S_{11}^* = (C_{22}^*C_{66}^* - C_{26}^{*2})/D \quad (113)$$

$$S_{22}^* = (C_{11}^*C_{66}^* - C_{16}^{*2})/D \quad (114)$$

$$S_{12}^* = (C_{16}^*C_{26}^* - C_{12}^*C_{16}^*)/D \quad (115)$$

$$S_{66}^* = (C_{11}^*C_{22}^* - C_{12}^{*2})/D \quad (116)$$

$$D = C_{11}^*C_{22}^*C_{66}^* - C_{12}^{*2}C_{66}^* \quad (117)$$

Following Equations 13 to 15 the Young's modulus and Poisson's ratio in the x-direction of the random-phase model are given by

$$E_x^* = 1/S_{11}^* \quad (118)$$

$$\nu_{xy}^* = -S_{12}^*/S_{11}^* \quad (119)$$

If the random-phase model is subjected to uniaxial tension, σ_x, the strain components are

$$\varepsilon_x = \sigma_x/E_x^* \quad (120)$$

$$\varepsilon_y = -(\nu_{xy}^*/E_x^*)\sigma_x \quad (121)$$

$$\gamma_{xy} = 0 \quad (122)$$

The strain of the fibre in its axial direction is calculated by substituting Equations 120–122 into Equation 99 and averaging over S (Equation 100)

$$\varepsilon_L^* = (\varepsilon_x - \varepsilon_y)F(k) + \varepsilon_y \quad (123)$$

where $F(k)$ is given by Equation 101.

5.2.3. Non-linear tensile stress–strain behaviour

The non-linear axial (x-direction) tensile stress–strain behaviour of the flexible composite is examined using the stepwise incremental analysis of Petit and Waddoups [42]. Consider an incremental tensile strain, Δe_x, applied on either the iso-phase or random-phase model. Here, $\Delta e_x = \Delta l/l$; Δl and l are the incremental length and the current length, respectively. Using the initial Young's modulus, E_x^*, the first stress increment, $\Delta\sigma_x$, is calculated by the linear elastic equation

$$\Delta\sigma_x = E_x^* \Delta e_x \quad (124)$$

where E_x^* is given by Equations 98 and 118 for the iso-phase and random-phase models, respectively. The nth stress increment is added to the previous stress state after $n - 1$ increments to determine the current total stress.

$$(\sigma_x)_n = (\sigma_x)_{n-1} + (\Delta\sigma_x)_n \quad (125)$$

For the iso-phase model, the average tensile strain increment of the fibre along its axial direction, Δe_L^*, is given by substituting Equation 124 into Equation 100

$$\Delta e_L^* = [(S_{11} - S_{12})F(k) + S_{12}]\Delta\sigma_x \quad (126)$$

For the random model, the transverse strain increment, Δe_y, is determined from Δe_x and v_{xy}^*

$$\Delta e_y = -v_{xy}^* \Delta e_x \quad (127)$$

Then, the tensile strain increment of the fibre is calculated by substituting Δe_x and Δe_y into Equation 123

$$\Delta e_L^* = (\Delta e_x - \Delta e_y)F(k) + \Delta e_y \quad (128)$$

The total strain, referring to the current specimen length, after n increments is

$$e_x = \sum_{i=1}^{n} \Delta e_x = \sum_{i=1}^{n} \frac{\Delta l}{l} \quad (129)$$

Replacing Δl by the infinitesimal increment, dl, we obtain

$$e_x = \int_{l_0}^{l} \frac{dl}{l} = \ln \frac{l}{l_0} = \ln(1 + \varepsilon_x) \quad (130)$$

Here, ε_x is the tensile strain referred to the initial specimen length, l_0:

$$\varepsilon_x = \frac{l - l_0}{l_0} \quad (131)$$

In the range of large strain, the use of ε_x is more convenient than the summation of Δe_x. From Equation 130

$$\varepsilon_x = \exp(e_x) - 1 \quad (132)$$

Then, the total strain, after the nth increment, in the axial direction (ε_x), transverse direction (ε_y) and in the fibre (ε_L^*) are given by

$$(\varepsilon_x)_n = \exp\left(\sum^{n} \Delta e_y\right) - 1 \quad (133)$$

$$(\varepsilon_y)_n = \exp\left(\sum^{n} \Delta e_y\right) - 1 \quad (134)$$

$$(\varepsilon_L^*)_n = \exp\left(\sum^{n} \Delta e_L^*\right) - 1 \quad (135)$$

Finally, the change of fibre shape under loading needs to be taken into account. Owing to the tensile loading in the x-direction, the wavelength of the curved fibre is changed to

$$\lambda = \lambda_0(1 + \varepsilon_x) \quad (136)$$

where λ and λ_0 are the current and initial values of the wavelength, respectively, and the total strain, ε_x, is given by Equation 133. The current value of the fibre length is

$$s = s_0(1 + \varepsilon_L^*) \quad (137)$$

where s_0 is the initial fibre length and ε_L^* is the total fibre strain given by Equation 135. In order to determine the shape of the fibre, it is assumed that the fibre maintains a sinusoidal waviness during deformation while varying its amplitude, a, and wavelength, λ. The current value of the amplitude, a, can be determined from Fig. 16 from the given current values of λ and s. The values of $k^2 = c/(1 + c)$, $c = (2\pi a/\lambda)^2$, E_x^* and v_{xy}^* after the nth step are determined from the current values of λ and a, and these values are used in the $(n + 1)$th step of the incremental analysis. Equations 125 and 133 give the uniaxial tensile stress/strain relation of the flexible composite.

5.2.4. Numerical examples

The elastic constants of fibres [3] and matrices [4] used in the numerical calculations are shown in Table I. Linear elastic stress–strain relations are assumed for glass and Kevlar fibres. Rubber elasticity [43, 44] is assumed for PBT and the other elastomeric polymers

$$\sigma = \frac{E_m^0}{3}\left(\alpha - \frac{1}{\alpha^2}\right) \quad (138)$$

where E_m^0 is the initial Young's modulus of the matrix, and α is the extension ratio

$$\alpha = 1 + \varepsilon_x \quad (139)$$

The secant Young's modulus of the matrix, E_m, is determined from the current tensile strain, ε_x (Equations 133 and 139)

$$E_m = \frac{d\sigma}{d\varepsilon_x} = \frac{E_m^0}{3}\left(1 + \frac{2}{\alpha^3}\right) \quad (140)$$

TABLE I Elastic constants and elongations [43, 44]

	E_L (GPa)	E_T (GPa)	G_{LT} (GPa)	ν_{LT}	ν_{TT}	ε_b (%)
Glass fibre	72.52		29.7	0.22		4
Kevlar	151.6	4.13	2.89	0.35	0.35	3.5
PBT matrix	2.156		0.77	0.4		50–300

Isotropic relation $G = E/2(1 + \nu)$ is assumed.
ε_0 = strain at break.

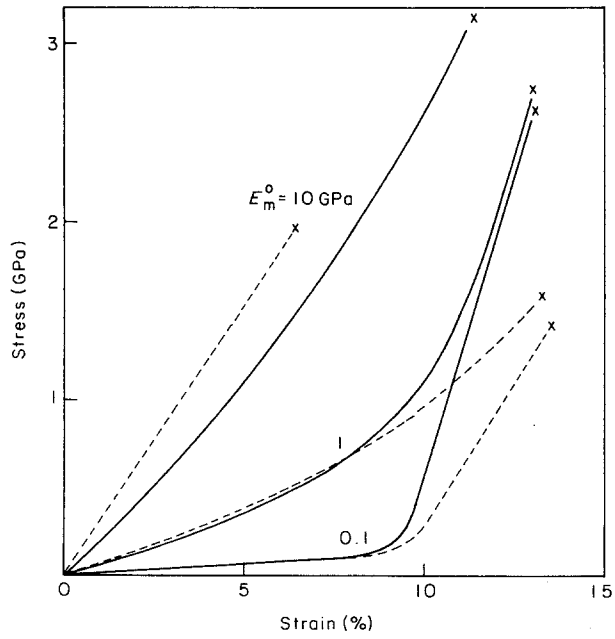

Figure 20 Comparison of the effects of (– – –) glass and (——) Kevlar fibres in an iso-phase composite at various E_m^0. Rubber elasticity is assumed for the matrix. (x) Average fibre axial tensile strain, ε_L^* reaches 4% and 3.5% for glass and Kevlar fibres, respectively. $v_m = 0.4$, $V_f = 50\%$, $a/\lambda = 0.1$ [1].

Numerical examples of the stress–strain relations predicted by the incremental analysis are shown in Figs 20 and 21. The results indicate that Kevlar is less effective than glass fibre in contributing to the stiffness of curved fibre composites, because the transverse Young's modulus of Kevlar is lower than that of glass. After the curved fibres are stretched, however, Kevlar becomes increasingly more effective to the stiffness and strength (Fig. 20). For a given curved fibre composite, the random phase model predicts higher Young's modulus and lower elongation than those of the iso-phase model (Fig. 21).

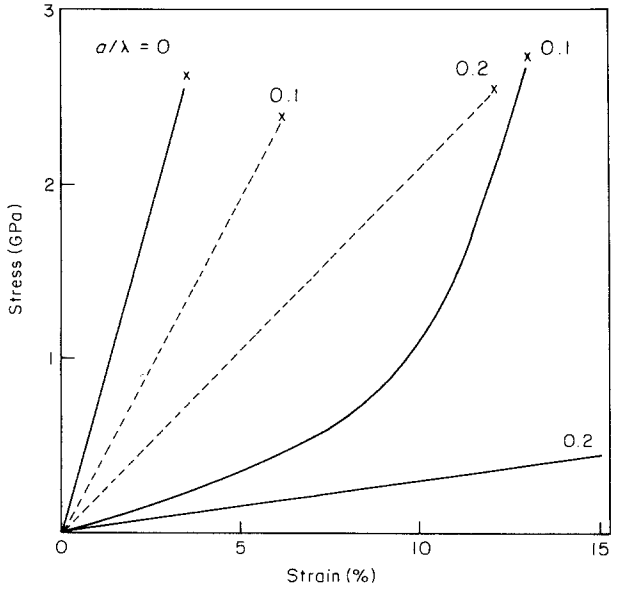

Figure 21 Tensile stress (σ_x)/strain(ε_x) curves of Kevlar/PBT polymer composites predicted by using the iso-phase (——) and random-phase (– – –) models. $E_m^0 = 1$ GPa, $v_m = 0.4$ and $V_f = 50\%$. (x) Average fibre axial tensile strain, ε_L^* reaches 3.5% [1].

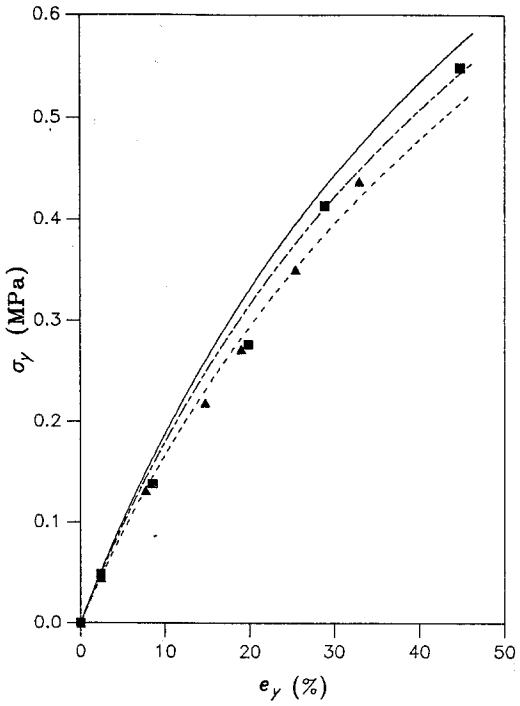

Figure 22 Comparisons between theoretical predictions and experimental data of transverse tension of an iso-phase model. Specimen initial $a/\lambda = 0.05$ to 0.07 and $V_f = 1.337\%$ for Thornel-300/silicone-elastomer composites. (▲) Specimen 1, (■) specimen 2, a/λ = (——) 0.03, (– –) 0.05, (– – –) 0.09.

5.3. Transverse tensile behaviour

The transverse tensile behaviour of curve fibre composites is analysed for both iso-phase and random-phase models. The lamination theory is the basis of the incremental analysis [45].

5.3.1. Iso-phase model

Consider the small volume element situated between y and $y + dy$ in the iso-phase model as shown in Fig. 17. It is assumed that the transverse stress, σ_y, is uniformly distributed along one wavelength λ. Then an element of the size $dydx$ can be treated as an off-axis unidirectional lamina. From Equation 32 and plane stress condition, the strain components developed in this element are

$$\varepsilon_x = S_{12}\sigma_y, \quad \varepsilon_y = S_{22}\sigma_y, \quad \gamma_{xy} = S_{26}\sigma_y \tag{141}$$

Then the transverse strain averaged over the wavelength of the iso-phase model is

$$\varepsilon_y^* = \frac{1}{\lambda}\int_0^\lambda \varepsilon_y \, dx \tag{142}$$

The effective Young's modulus in the y direction is

$$E_y^* = \frac{\sigma_y}{\varepsilon_y^*} = (1 + c)^{3/2}\Big/\left[((1 + c)^{3/2} - 1 - \tfrac{3}{2}c)S_{11} + \left(1 + \frac{c}{2}\right)S_{22} + \frac{c}{2}(2S_{12} + S_{66})\right] \tag{143}$$

Following the approach of Section 5.2.1, the average tensile strain along the fibres due to transverse tension is obtained by substituting Equation 141 into Equation 99 and averaging over the length s.

$$\varepsilon_L^* = [(S_{12} - S_{11})F(k) + S_{11}]\sigma_y \tag{144}$$

$F(k)$ is given by Equation 101.

Kuo *et al.* [45] also analysed the transverse tensile behaviour based upon the constant strain assumption. This assumption is validated by the observation during transverse tension experiments that the elongation of the specimen is uniform throughout its width away from the specimen ends. Although the constitutive relations are not of the same form for constant stress and constant strain analyses, the numerical calculations in [45] yield the same result. This is the direct consequence of the approaches, namely, the stress (or strain) is considered in the average sense along the x-direction.

5.3.2. Random-phase model

The transverse Young's modulus and minor Poisson's ratios are given by

$$E_y^* = 1/S_{22}^* \quad (145)$$

$$\nu_{yx}^* = -S_{12}^*/S_{22}^* \quad (146)$$

Under the transverse stress, σ_y, the strain components are

$$\varepsilon_x = -(\nu_{yx}^*/E_y^*)\,\sigma_y \quad (147)$$

$$\varepsilon_y = \sigma_y/E_y^* \quad (148)$$

$$\gamma_{xy} = 0 \quad (149)$$

Again, the average tensile strain along the fibre is obtained from Equation 123.

5.4. Experiments

The experimental material system reported by Kuo *et al.* [45] is based upon Sylgard 184 silicone elastomer reinforced with Thornel – 300 carbon fibre. A loose fibre bundle contains 1000 filaments, with a filament diameter of 7 μm. The matrix properties are given in Table II. The specimen fabrication technique follows that given in [46].

Fig. 22 depicts the comparison between theoretical curves and experimental data of an iso-phase model under transverse tension. The initial a/λ values of the specimens are in the range 0.05 to 0.07. The fibre volume fraction is very low, i.e. 1.337%.

6. Non-linear elastic behaviour–finite deformation

The incremental analysis of Section 5 is based upon the assumption of superposition of infinitesimal linear elastic deformation. Thus, the technique should be considered as an approximation. The general non-linear theory of anisotropic material has been studied previously [47, 48]. However, in the treatment of non-linear problems, difficulties often arise in the analytical determination of the response function [49]. In some of the existing composite analyses, the non-linear stress–strain curves in the principal material directions are determined experimentally. A number of methods and various response functions have been adopted to represent these curves [17, 49–51]. However, the geometric non-linearity, which is important in the analysis of flexible composites, is not emphasized in these studies. The influence of the geometric change of fibres has been summarized and studied by the theory of ideal fibre-reinforced material [52]. There, the kinematic constraints are substituted for the material stress–strain relations by assuming that the fibres are inextensible.

In order to treat the finite deformation problem, Luo and Chou [46] has developed a constitutive model based upon the Eulerian description. The material non-linear stress–strain relation including the stretching–shear coupling is derived by using the stress energy density referring to the deformed volume. The geometric non-linear behaviour, due to fibre reorientation is analysed through an iterative calculation procedure. The analytical predictions of finite elastic deformations for tyre cord/rubber and Kevlar/silicone-elastomer flexible composite are compared with experimental data.

TABLE II Measured properties of SYLGARD 184 silicone elastomer [45]

Initial Young's modulus, E^0 (MPa)	1.7
Shear rigidity, G (MPa)	0.582*
Poisson's ratio, ν	0.46
Maximum breaking strain (%)	50–100

*Isotropic relation $G = E/2(1 + \nu)$ is assumed.
ε_b = strain at break.

6.1. Eulerian strains and finite deformation

Both the Lagrangian and Eulerian descriptions have been used in the theory of finite elasticity [53]. The strain tensor associated with the Lagrangian system (Lagrangian strain, E_{ij}) is known as Green's strain tensor. The strain tensor associated with the Eulerian system (Eulerian strain, e_{ij}) is known as Almansi's strain tensor for large deformation and Cauchy's strain tensor for infinitesimal deformation.

In a rectangular Cartesian coordinate system x_i, the Eulerian strains are expressed as

$$e_{ij} = 1/2(u_{i,j} + u_{j,i} - u_{\alpha,i}u_{\alpha,j}) \quad (150)$$

where u_i denotes the displacement in the x_i direction. In the two-dimensional case

$$e_{11} = \frac{\partial u_1}{\partial x_1} - \frac{1}{2}\left[\left(\frac{\partial u_1}{\partial x_1}\right)^2 + \left(\frac{\partial u_2}{\partial x_1}\right)^2\right] \quad (151)$$

$$e_{22} = \frac{\partial u_2}{\partial x_2} - \frac{1}{2}\left[\left(\frac{\partial u_1}{\partial x_2}\right)^2 + \left(\frac{\partial u_2}{\partial x_2}\right)^2\right] \quad (152)$$

$$e_{12} = \frac{1}{2}\left(\frac{\partial u_1}{\partial x_2} + \frac{\partial u_2}{\partial x_1} - \frac{\partial u_1}{\partial x_1}\frac{\partial u_1}{\partial x_2} - \frac{\partial u_2}{\partial x_1}\frac{\partial u_2}{\partial x_2}\right) \quad (153)$$

For a composite lamina under finite deformation, the fibre orientation generally deviates significantly from its initial position. The Lagrangian description of such deformation is considered first. In Fig. 23a, the initial fibre orientation is at an angle θ_0 with respect to the x-axis. The Cartesian coordinates l–t coincide with the initial principal material directions; namely, l and t are along the fibre and transverse directions, respectively. Under loading, the rectangular element ABCD is changed into a quadrilateral element A′B′C′D′. There is an angle $\Delta\theta$ between AD and A′D′. Corresponding to this change, the current fibre orientation

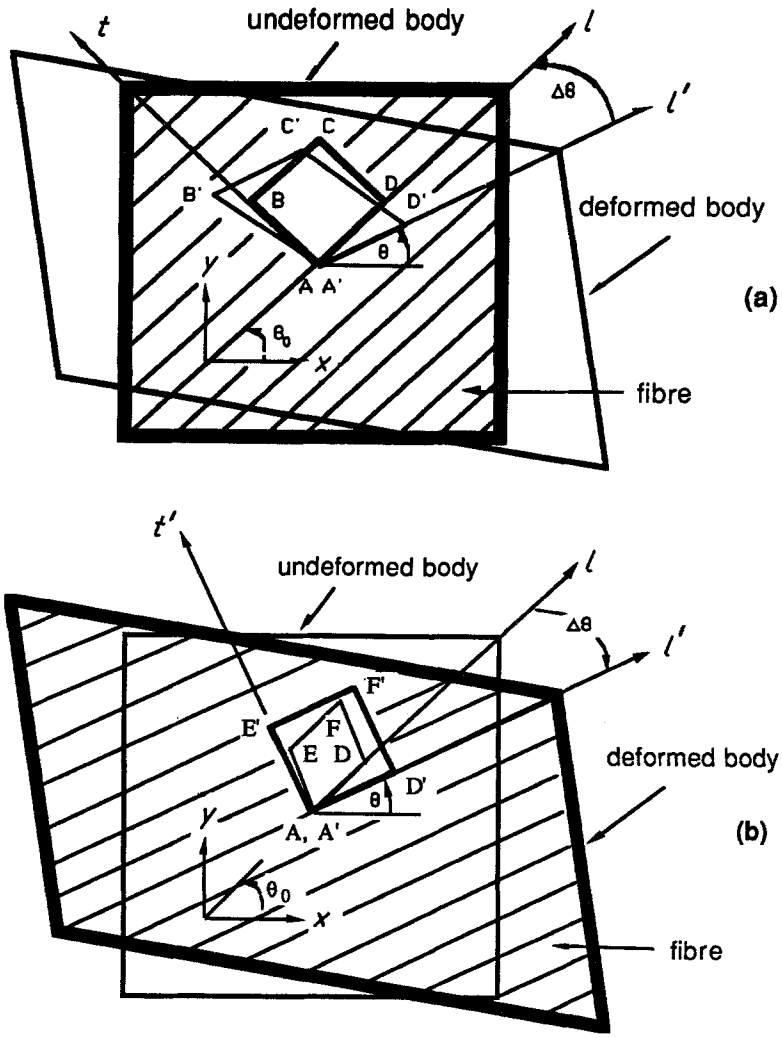

Figure 23 A rectangular element of composite lamina before and after loading, referring to (a) the Lagrangian system, (b) the Eulerian system.

l' is at an angle θ with respect to the x-axis, and

$$\theta = \theta_0 + \Delta\theta \tag{154}$$

The change of fibre orientation not only alters the geometric configuration of the lamina, but also the elastic properties with respect to the initial coordinate system. All these effects need to be considered for the prediction of the stress–strain relation. Thus, it is very cumbersome to investigate such changes based on the Lagrangian system.

In the analysis of Luo and Chou [46], the Eulerian description is adopted, and the rectangular element A′E′F′D′ in the deformed body of Fig. 23b is considered. The sides A′D′ and A′E′ coincide with the Cartesian coordinates l'–t', with l' referring to the current fibre direction. Thus, the quadrilateral element AEFD corresponds to the rectangular element A′E′F′D′ in the undeformed state. One may assume that the rectangle A′E′F′D′ undergoes two stages of deformation in being restored to its initial shape AEFD. These stages are illustrated in Fig. 24. First, A′E′F′D′ becomes a smaller rectangle A″E″F″D″ by removing the normal stresses; then it reverses to AEFD by removing the shear stress. Obviously, γ_{12} is the angular deviation from a right-angle in the undeformed lamina between two intersecting line elements which coincide with the coordinates l'–t' in the deformed lamina.

The deformations depicted in Fig. 24 can be related to the Eulerian strain components. Let the line elements AD = dl_0 and AE = dt_0 in the undeformed lamina (Fig. 24c); also define A′D′ = dl and A′E′ = dt in the deformed lamina (Fig. 24a). Then, the physical significance of the Eulerian strains can be explained as

$$\frac{(dl)^2 - (dl_0)^2}{(dl)^2} = 2e_{11} \tag{155}$$

$$\frac{(dt)^2 - (dt_0)^2}{(dt)^2} = 2e_{22} \tag{156}$$

$$\sin\gamma_{12} = \frac{2e_{12}}{[(1 - 2e_{11})(1 - 2e_{22})]^{1/2}} \tag{157}$$

Here, the subscripts 1 and 2 refer to the l' and t' directions, respectively. Let the axial "engineering strain" be defined as

$$\varepsilon_1 = \frac{dl - dl_0}{dl_0} \tag{158}$$

Then, it follows that

$$\varepsilon_1 = (1 - 2e_{11})^{-1/2} - 1 \tag{159}$$

and

$$e_{11} = [1 - (1 + \varepsilon_1)^{-2}]/2 \tag{160}$$

6.2. Constitutive relations

Luo and Chou [46] considered the stress energy per unit area of the deformed lamina, and adopted the following polynomial expression for the plane-stress

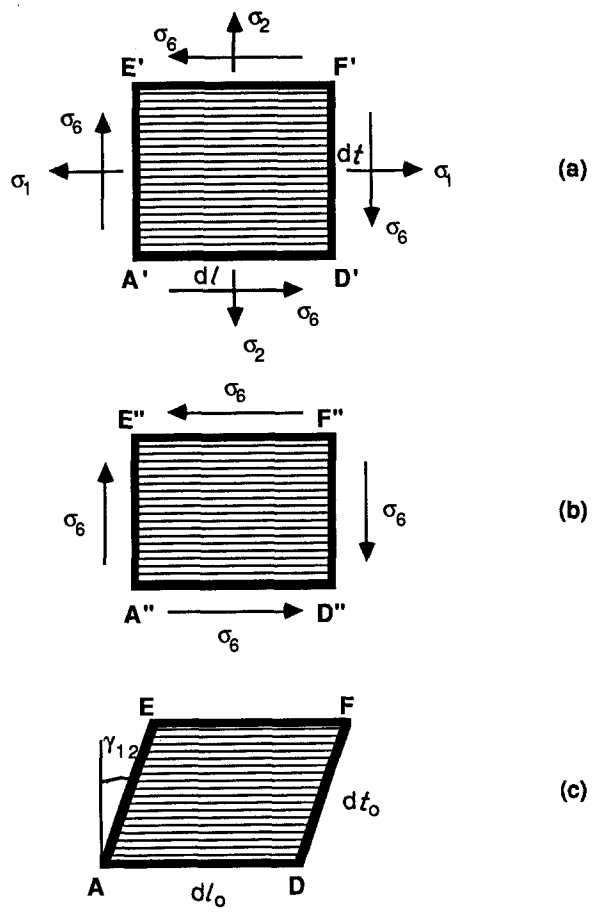

Figure 24 Illustration of the deformation of a unidirectional rectangular element in the Eulerian system.

complementary energy function in the Eulerian system, in terms of σ_1, σ_2 and σ_6^2.

$$W^* = (1/2)S_{11}\sigma_1^2 + (1/3)S_{111}\sigma_1^3 + (1/4)S_{1111}\sigma_1^4 + S_{12}\sigma_1\sigma_2 + (1/2)S_{22}\sigma_2^2 + (1/3)S_{222}\sigma_2^3 + (1/4)S_{2222}\sigma_2^4 + (1/2)S_{66}\sigma_6^2 + (1/4)S_{6666}\sigma_6^4 + S_{166}\sigma_1\sigma_6^2 + S_{2266}\sigma_2^2\sigma_6^2 \quad (161)$$

Again, the subscripts 1 and 2 refer, respectively, to the l' and t' directions in Fig. 23b. Also, the short-handed notations are used, namely, $\sigma_1 = \sigma_{11}$, $\sigma_2 = \sigma_{22}$, and $\sigma_6 = \sigma_{12}$. S_{ij}, S_{ijk} and S_{ijkl} are the compliance constants.

By using the relation

$$e_i = \frac{\partial W^*}{\partial \sigma_i} \quad (162)$$

the following constitutive equations for the rectangular element A'E'F'D' (Fig. 24) in the Eulerian system are obtained.

$$e_1 = S_{11}\sigma_1 + S_{111}\sigma_1^2 + S_{1111}\sigma_1^3 + S_{12}\sigma_2 + S_{166}\sigma_6^2 \quad (163)$$

$$e_2 = S_{22}\sigma_2 + S_{222}\sigma_2^2 + S_{2222}\sigma_2^3 + S_{12}\sigma_1 + 2S_{2266}\sigma_2\sigma_6^2 \quad (164)$$

$$e_6 = S_{66}\sigma^6 + S_{6666}\sigma_6^3 + 2S_{166}\sigma_1\sigma_6 + 2S_{2266}\sigma_2^2\sigma_6 \quad (165)$$

Here $e_1 = e_{11}$, $e_2 = e_{22}$, and $e_6 = 2e_{12}$. The choice of compliance constants in Equation 161 is made on the following basis. First, the terms S_{11}, S_{22}, S_{12} and S_{66} are needed for the linear deformation. Second, the terms S_{111} and S_{222} are adopted for representing the bimodular behaviour in the axial and transverse directions, respectively. Third, the non-linear terms are given by S_{1111}, S_{2222} and S_{6666}. Lastly, the greatest uncertainty involves the coupling terms between the normal and the shear deformations. Unlike in rigid composites, the coupling effects may not be negligible in flexible composites. Two terms, S_{166} and S_{2266}, are retained to represent the interactions between axial and shear deformations.

Equations 163 to 165 are similar to Hahn and Tsai's expressions [49] in their mathematical forms. However, there are some basic differences: (a) the strains on the left-hand side of Equations 163 to 165 are Eulerian strains; (b) the stresses on the right-hand side of these equations act on a rectangular element in the deformed body; and (c) the coordinates l'–t' depend on the deformation, and the configuration of this element in the undeformed body is initially "unknown".

The compliance constants in Equations 163 to 165 can be determined experimentally. The second-order constants (S_{11}, S_{22}, S_{12} and S_{66}) are based on linear theory. The other constants are obtained by fitting the theoretical curves with experimental data. For example, when $\sigma_1 \neq 0$ and $\sigma_2 = \sigma_6 = 0$, Equation 163 becomes

$$e_1 = S_{11}\sigma_1 + S_{111}\sigma_1^2 + S_{1111}\sigma_1^3 \quad (166)$$

The nonlinear σ_1–e_1 curve can be obtained from simple experiments. Then, S_{11} is obtained from the initial slope of the experimental curve (i.e. $S_{11} = 1/$ Young's modulus). S_{111} (which reflects bimodular behaviour) and S_{1111} are determined by fitting the theoretical curves to both tension and compression experimental data. The shear and stretching–shear coupling terms can be obtained from off-axis tensile tests with various initial fibre orientations, and the stress–strain relation expressed in terms of the x–y coordinate system in the general form.

$$[e] = [S^*][\sigma] \quad (167)$$

Details of $[S^*]$ can be found in [46].

6.3. Reorientation of fibres

The fibre reorientation due to finite deformation has been predicted as follows. First, the angles DAD' and EAE' are defined as α and β, respectively, in Fig. 23b. Then,

$$\Delta\theta = (\alpha + \beta)/2 + (\alpha - \beta)/2 \quad (168)$$

$(\alpha + \beta)/2$, the symmetric part of $\Delta\theta$, equals $\gamma_{12}/2$. From Equation 157

$$\gamma_{12} = \sin^{-1}\left[\frac{2e_{12}}{[(1 - 2e_{11})^{1/2}(1 - 2e_{22})^{1/2}}\right] \quad (169)$$

where, e_{11}, e_{22} and e_{12} can be determined from Equations 163 to 165. $(\alpha - \beta)/2$, the antisymmetric part of $\Delta\theta$, is defined as ω. It is understood that ω is the rigid body rotation, which is independent of the coordinate system but dependent on the boundary

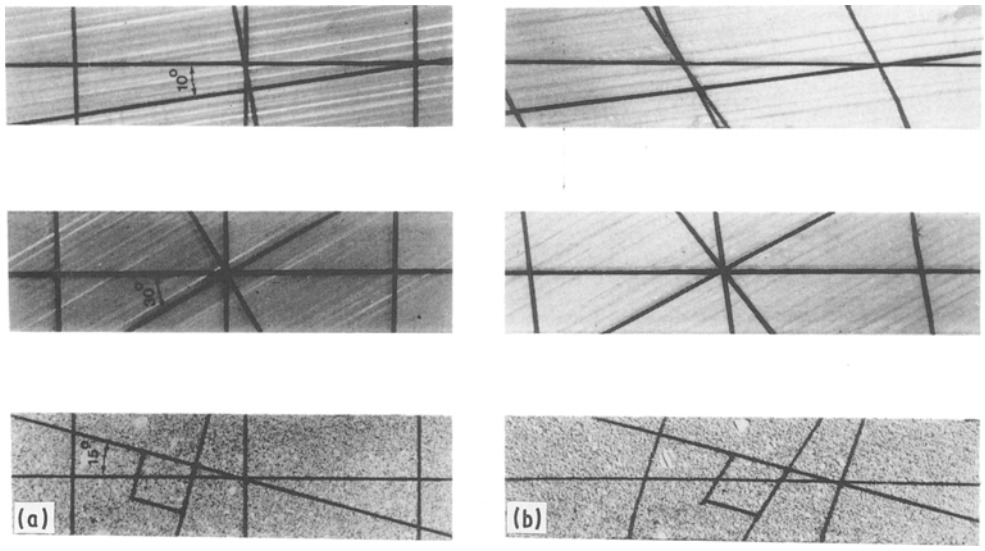

Figure 25 Off-axis specimens of elastomeric composite laminae (a) without loading, (b) with loading. The 15° specimen is a tyrecord/rubber composite, and the 10° and 30° specimens are Kevlar/silicone composites.

conditions. Then Equation 168 can be rewritten as

$$\Delta\theta = \frac{\gamma_{12}}{2} + \omega \tag{170}$$

From Equations 154, 167 and 170, the current strains and fibre orientations can be determined by an iterative calculation technique [46]. The determination of ω is demonstrated in Section 6.5.

6.4. Experiments

6.4.1. Materials, fabrication and tests

Experiments have been conducted by Luo and Chou [46] to study the non-linear elastic behaviour of composites under finite strain. Two types of flexible composites are selected for the experimental work. One is the tyre cord/rubber sheet widely used in the tyre industry. The other is Kevlar-49/silicone-elastomer lamina. The fibre material used in the fabrication is Kevlar-49, 1420 denier (1 denier = 19/9000 m) with 1000 filaments in a yarn. The resin is Sylgard 184 silicone elastomer. The resin is transparent and has an elongation up to 100%.

The unidirectional composite laminae are made by a frame winding method [54]. The curing process is performed in air or in an autoclave. The procedure of making flexible composite laminae with wavy fibres is basically the same as that for making unidirectional fibre laminae, except that the pre-coated fibres are pressed by a mould to form a pre-designed shape. Then, these wavy fibres are aligned and embedded in the resin.

Luo and Chou [46] performed longitudinal, transverse, and off-axis tensile tests on unidirectional fibre specimens. For wavy fibre specimens, only longitudinal properties are measured. The measurement of large strain is performed using extensometers with a single-point edge knife for the unidirectional fibre specimen, and a photographic method for the wavy fibre specimens.

The experimentally determined elastic properties of tyre cord/rubber and Kevlar/silicone-elastomer are listed in Table III.

6.5. Numerical examples

Luo and Chou [46] performed numerical calculations for (1) unidirectional off-axis laminae and (2) a lamina with sinusoidally shaped fibres. Uniaxial loading is applied (i.e. $\sigma_{xx} \neq 0$, $\sigma_{yy} = \sigma_{xy} = 0$). The total Eulerian strains and the current fibre orientation are calculated from Equations 154, 167 and 170 by an iterative trial-and-error technique.

6.5.1. Unidirectional off-axis laminae

The elastic properties of the experimental materials are given in Table III. Figs 25a and b are photographs of the off-axis specimens without and with loading, respectively. Fig. 25b shows that the central lines of specimens remain straight under loading. Thus, the rigid body rotation in Equation 170 can be expressed as

$$\omega = -\frac{\gamma_{xy}}{2} \tag{171}$$

where γ_{xy} is the angular deviation from a right-angle in the undeformed lamina between two line elements which coincide with the coordinates x–y in the deformed lamina. From Equation 157

$$\gamma_{xy} = \sin^{-1}\left\{\frac{2e_{xy}}{(1 - 2e_{xx})^{1/2}(1 - 2e_{yy})^{1/2}}\right\} \tag{172}$$

Fig. 26 shows the comparisons between analytical predictions and experimental results for off-axis

TABLE III Elastic properties of elastomeric composite laminae

	Tyre cord/rubber	Kevlar-49/elastomer (V_f = 9%)
S_{11} (MPa)$^{-1}$	0.165E-3	0.114E-3
S_{1111} (MPa)$^{-3}$	0	0
S_{12} (MPa)$^{-1}$	−65.9E-6	−69.9E-6
S_{22} (MPa)$^{-1}$	0.121	0.306
S_{2222} (MPa)$^{-3}$	51.4E-3	0.563
S_{66} (MPa)$^{-1}$	0.408	0.387
S_{6666} (MPa)$^{-3}$	0.183	77.5E-3
S_{166} (MPa)$^{-2}$	0.131E-3	3.43E-6
S_{2266} (MPa)$^{-3}$	0.469	56.3E-3

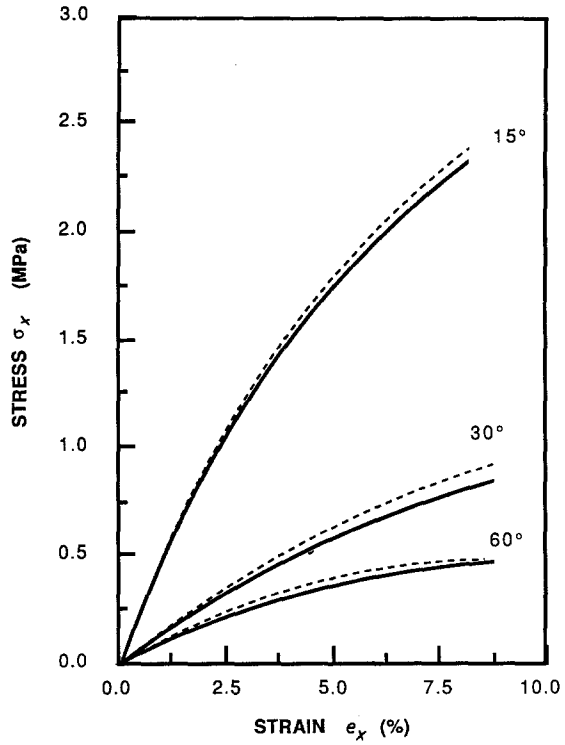

Figure 26 Comparisons between (——) theoretical curves and (– – –) experimental results on 15°, 30°, and 60° off-axis stress–strain responses of tyrecord/rubber composite laminae.

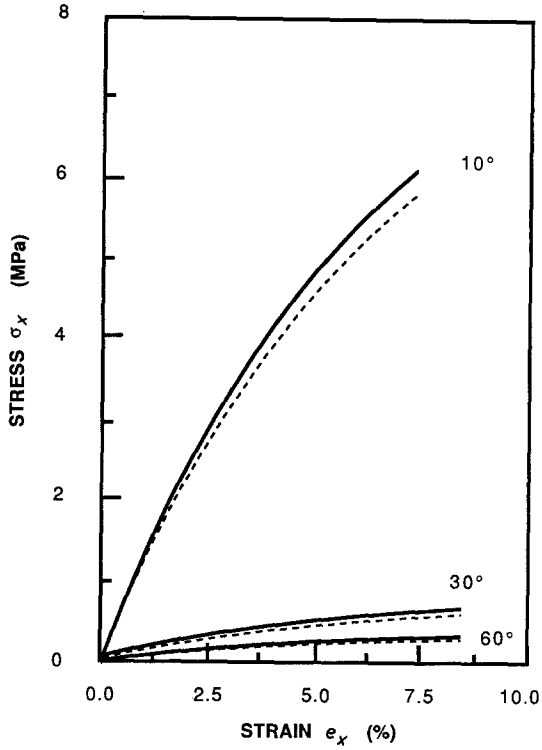

Figure 27 Comparisons between (——) theoretical predictions and (– – –) experimental results on 10°, 30°, and 60° degree off-axis stress–strain responses of Kevlar-49/silicone-elastomer composite laminae.

responses of tyre cord/rubber composites. The fibre initial orientations are 15°, 30° and 60°. The maximum strains are over 6%. The same comparisons for Kevlar-49/silicone-elastomer specimens are shown in Fig. 27. The fibre initial orientations are 10°, 30°, and 60° in this case. Good correlations have been found.

6.5.2. Flexible composite specimens with wavy fibres

Fig. 28 illustrates the deformations of a flexible composite sample with wavy fibres under different levels of loading. Fig. 29 is a photoelastic view of a flexible composite sample under longitudinal loading, which shows that relatively uniform strain is maintained in distinct regions along the x-axis.

The deformation of this flexible composite is best understood by examining a representative element of the wavy fibre which contains a half-wave of the sinusoidal curve (Fig. 30). This element can be divided into sub-elements along the x-axis. Then, its longitudinal deformation is the summation of the deformations of all of these sub-elements. Luo and Chou [46] divided the fibre element into three regions along the x-axis denoted by AB, CD and BC. In the regions AB and CD, the fibre segments are considered to be parallel to the x-axis. Let AB + CD = a. In the region BC, the fibre is assumed to have an average inclination angle of θ_0 with respect to the x-axis in the initial state; also BC = b. Then, the overall "engineering strain" of the

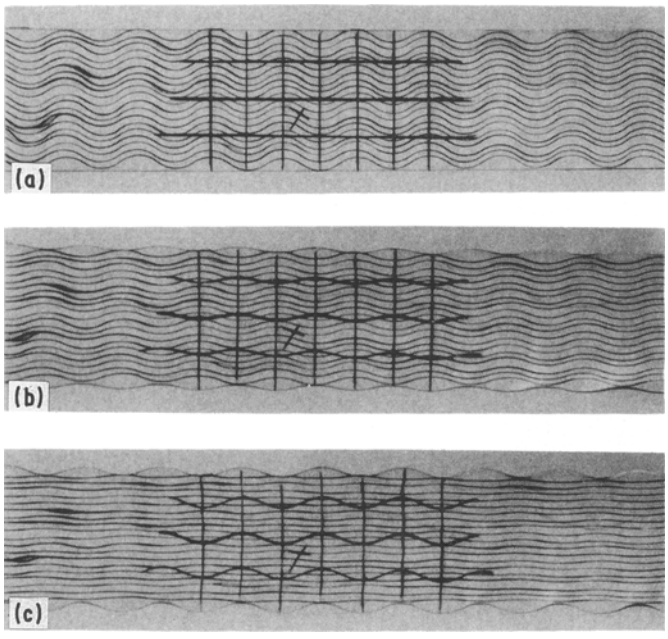

Figure 28 Photographs of a flexible composite lamina sample (graphite/silicone-elastomer) with sinusoidally shaped fibres for loads at (a) 0 kg, (b) 6 kg, and (c) 20 kg.

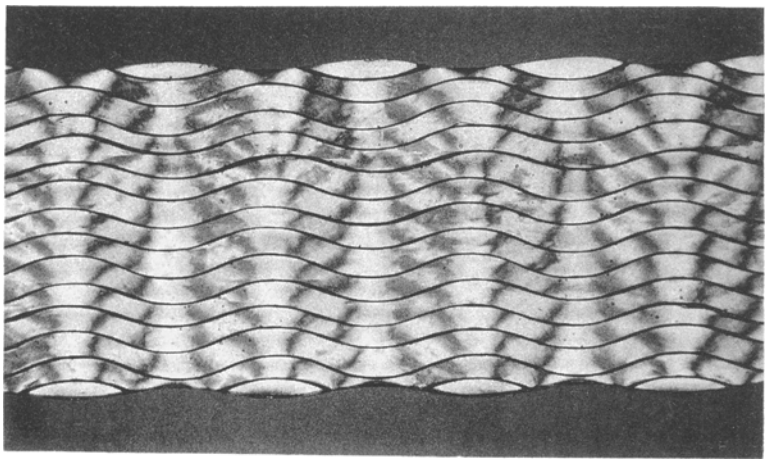

Figure 29 The photoelastic view of a flexible composite lamina (graphite/photostress material PL-2) with sinusoidally shaped fibres.

specimen in the x-direction is

$$\varepsilon_x = \varepsilon_a[a/(a + b)] + \varepsilon_b[b/(a + b)] \quad (173)$$

Here, ε_a is the strain in the AB and CD regions, which is obtained from Equations 159, 160 and 167 by setting $\theta = 0$. ε_b is the average strain of the region BC, which is treated as an off-axis lamina. Referring to Equation 158, ε_b is defined as

$$\varepsilon_b = \frac{L \cos \theta - L_0 \cos \theta_0}{L_0 \cos \theta_0}$$

$$= \frac{\cos \theta}{(1 - 2e_{11})^{1/2}(\cos \theta_0 - 1)} \quad (174)$$

where L and θ are respectively, the instantaneous values of L_0 and θ_0.

In this wavy fibre composite, the central line of the specimen does not remain straight under loading, but the lines BB′ and CC′ remain perpendicular to the x-axis as shown in Figs 28 and 29. Thus

$$\omega = \frac{\gamma_{xy}}{2} \quad (175)$$

Fig. 31 shows the theoretical and experimental relation of longitudinal stress, σ_x versus average strain, ε_x of the flexible composite specimens. The initial fibre orientation angle θ_0 in the off-axis part BC is in the range of 19° to 28°. Thus, the average value $\theta_0 = 23.5°$ has been assumed. The theoretical curves are obtained for $\theta_0 = 19°$, 23.5°, and 28°. The experimental strain values of ε_x are obtained by the photographic method. The agreement between theory and experiment is good.

6.6. Comparison with other theories

Recently, Luo and Chou [55] developed an alternative modelling technique based upon the Lagrangian description. In this work the constitutive equations for flexible composites are derived based upon a strain-energy density expression which is assumed to be a function of the Lagrangian strain components referring to the initial principal material coordinates.

Fig. 32 shows a comparison of the three theoretical approaches discussed in this review and based upon the Lagrangian description (theory 1), Eulerian description (theory 2) and the incremental analysis (theory 3). Experimental data are from the Kevlar/silicone system given in Section 6.4. The theoretical predictions appear to be more sensitive to the models at lower stress level.

7. Concluding remarks

This review article examines three types of flexible composites: cord/rubber composites, coated fabrics, and composites composed of wavy fibres. The following observations and conclusions are pertinent.

1. The lamination theory is adequate in describing the linear elastic stress–strain relations of flexible composites under small deformation.

2. The incremental analysis based upon superpositions of infinitesimal deformation can be used to approximate the non-linear elastic stress–strain relation of flexible composites. The validity and limitation of this approach should be assessed with care.

3. The non-linear theories of Luo, Rivlin and Chou based upon either the Eulerian or Lagrangian description appear to be most powerful in predicting the finite deformation of flexible composites.

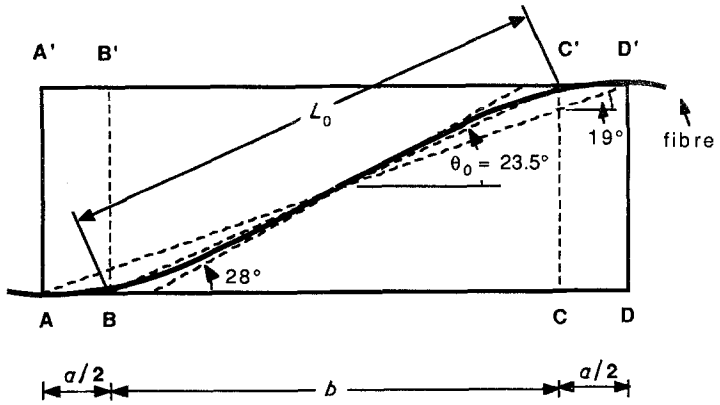

Figure 30 The original shape of a wavy fibre in a flexible composite specimen.

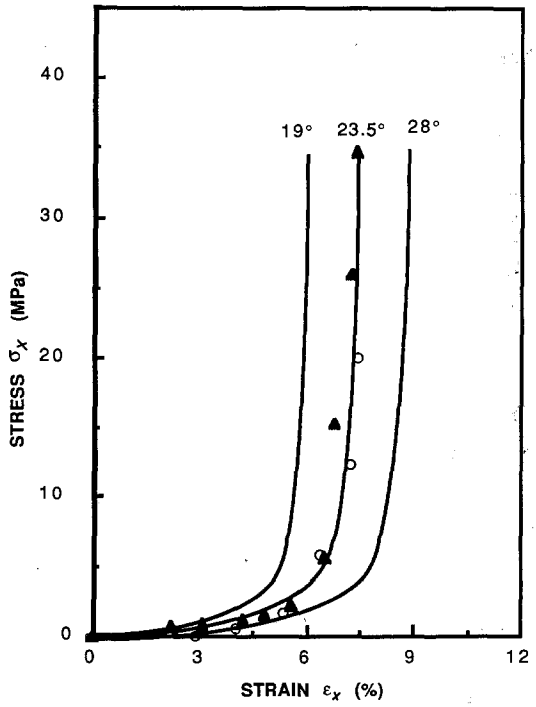

Figure 31 Stress σ_x plotted against overall average strain, ε_x for a flexible composite specimen with wavy fibres. (▲) Specimen 1, (○) specimen 2, (——) theory.

4. The better understanding of the behaviour of flexible composites requires the further development of (i) experimental techniques for monitoring large deformation, (ii) analytical technique for predicting inelastic behaviour, and (iii) modelling of damage and failure behaviour in general.

5. The stiffness, elongation to failure, energy absorbing capability, etc., of flexible composites can be tailor-made to suit specific applications through the judicious selection of fibre and matrix material systems and the design of fibre geometric configurations.

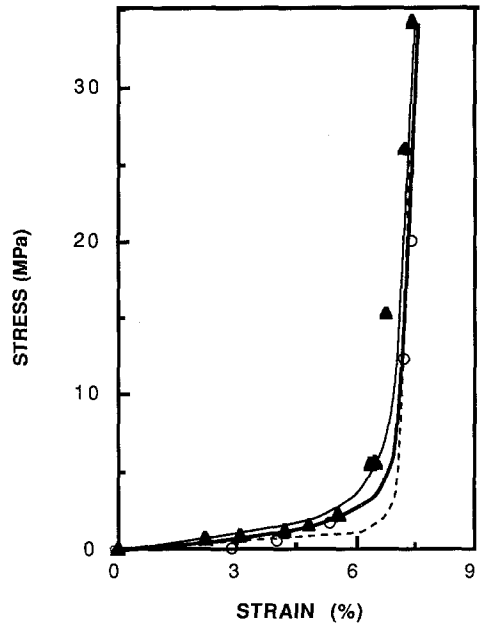

Figure 32 Stress (load/original cross-section area)–strain (increment in length/original length) relations of Kevlar-49/silicone-elastomer composite containing sinusoidally shaped fibres for $a/\lambda = 0.09$. Theory 1 (——) Lagrangian description; theory 2, (——) Eulerian description; theory 3, (– – –) incremental analysis, (▲), (○) experimental results.

Further optimization of composite performance can be achieved through fibre and/or matrix hybridization.

6. The potential of flexible composite applications in load-bearing structures, biomedical components, and robotics, just naming a few, is not fully realized. With the advent of analytical techniques, further innovative applications of flexible composites are feasible.

Acknowledgements

The author thanks the National Science Foundation for partial support through the Engineering Research Center for Composites Manufacturing Science and Engineering at the University of Delaware. The assistance of Messrs Joonhyung Byun, Li-Ning Yao and Shen-Yi Luo in the preparation of the manuscript is greatly appreciated.

References

1. T. W. CHOU and K. TAKAHASHI, *Composites* **18** (1987) 25.
2. S. Y. LUO and T. W. CHOU, "Modelling of the Nonlinear Elastic Behaviour of Elastomeric Flexible Composites", (Paper presented at American Chemical Society Meeting, Anaheim, California, September 1986).
3. J. D. WALTER, *Rubber Chem. Technol.* **51** (1978) 524.
4. F. MARTIN, *Jahrb. Dtsch. Luftfahrt-Forsch.* **1** (1939) 470.
5. S. K. CLARK, *Rubber Chem. Technol.* **37** (1964) 1365.
6. *Idem, Text Res. J.* **33** (1963) 295.
7. *Idem, ibid.* **33** (1963) 935.
8. V. E. GOUGH, *Rubber Chem. Technol.* **41** (1968) 988.
9. *Idem, Kautsch. Gummi. Kunstst.* **20** (1967) 469.
10. T. AKASAKA, Various Reports/Bulletins, Faculty of Science and Engineering, Chuo University, Tokyo (1959–64).
11. V. I. BIDERMAN, R. L. GUSLITSER, S. P. SAKHAROV, B. V. NENAKHOV, I. I. SELEZNEV, and S. M. TSUKERBERG, "Automobile Tires, Construction, Design, Testing and Usage", NASA, TT F-12, 382 (1969) (Original publication in Russian, State Scientific and Technical Press for Chemical Literature, Moscow, 1963).
12. V. A. ALLEY and R. W. FAIRLON, *J. Aircraft* **9** (1972) 55.
13. H. W. REINDHARDT, *Exp. Mechan.* **11** (1976) 71.
14. J. SKELTON, *J. Mat. J.M.L.S.A.* **6** (1971) 656.
15. N. STUBBS and S. THOMAS, "A Nonlinear Elastic Constitute Model for Coated Fabrics", "Mechanics of Material, 3" (Elsevier, North-Holland, 1984) pp. 157–168.
16. T. AKASAKA and N. YOSHIDA, in Proceedings of the International Conference on Mechanical Behavior of Materials, Koyto, Japan, Vol. 5 (1972) pp. 187–197.
17. T. ISHIKAWA and T. W. CHOU, *J. Compos. Mater.* **17** (1983) 399.
18. T. W. CHOU, "Proceedings of the First European Conference on Composite Materials", Bordeaux, France, (1985) pp. 133–138.
19. T. W. CHOU and J. M. YANG, *Met. Trans. A* **17A** (1986) 1547.
20. J. E. ASHTON, J. C. HALPIN and P. H. PETIT, "Primer on Composite materials: Analysis" (Technomic, Stamford, Connecticut, 1969).
21. J. R. VINSON and T. W. CHOU, "Composite Materials and Their Use in Structures" (Elsevier-Applied Science, London, 1975).
22. R. M. JONES, "Mechanics of Composite Materials" (McGraw-Hill, New York, 1975).
23. S. W. TSAI and H. T. HAHN, "Introduction to Composite Materials" (Technomic, Westport, Connecticut, 1980).
24. L. A. CARLSSON and R. B. PIPES, "Experimental Characterization of Advanced Composite Materials" (Prentice-Hall, Englewood Cliffs, New Jersey, 1987).
25. B. W. ROSEN, *Composites* **4** (1973) 16.

26. S. K. CLARK, "The Role of Textiles in Pneumatic Tyres" in "Mechanics of Flexible Fibre Assemblies, edited by J. W. S. Hearle, J. J. Thwaites and J. Amirbayat (Sijthoff and Noordhoff, The Netherlands, 1980) p. 471.
27. J. W. S. HEARLE, P. GROSBERG and S. BACKER, "Structural Mechanics of Fibers, Yarns and Fabrics" Vol. 1 (Wiley Interscience, New York, 1969).
28. J. E. ADKINS and R. S. RIVLIN, *Phil. Trans. Roy. Soc. London* **A248** (1955) 201.
29. T. AKASAKA, "Flexible Composites", in "Textile Structural Composites", edited by T. W. Chou and F. Ko (Elsevier Science, The Netherlands) in press.
30. J. D. WALTER, G. N. AVGEROPOULOS, M. L. JANSSEN and G. R. POTTS, *Tire Sci. Technol.* **1** (1973) 210.
31. J. D. WALTER and H. P. PATEL, *Rubber Chem. Technol.* **52** (1979) 710.
32. T. AKASAKA and M. HIRANO, *Comp. Mater. Structures* **1** (1972) 70.
33. S. K. CLARK, *Textile Res. J.* **33** (1963) 295.
34. F. BOHM, *Ing-Arch.* **35** (1966) 82.
35. A. Y. C. LOU and J. D. WALTER, "Interlaminar Shear Strain Measurements in Cord–Rubber Composites", paper presented at SESA meeting, Wichita, Kansas, May 1978.
36. R. G. PATTERSON, *Rubber Chem. Technol.* **42** (1969) 812.
37. S. K. CLARK and R. N. DODGE, "A Load Transducer for Tire Cord", Society of Automotive Engineers Paper no. 690 521 (1969).
38. J. D. WALTER and G. L. HALL, "Cord Load Characteristics in Bias and Belted-Bias Tires", Society of Automotive Engineers Paper no. 690 522 (1969).
39. "Stresses and Strains in Textile Structures", Shirley Institute Conference, 12 to 13 September 1973, Shirley Institute Publication S-10.
40. C. W. BERT and M. KUMAR, "Experiments on Highly Nonlinear Elastic Composites", in Proceedings NCKU/AAS International Symposium in Engineering Science and Mechanics, National Chen Kung University, Taiwan, Vol. 2, (Tainan, Taiwan, 1981) pp. 1269–83.
41. C. W. BERT and J. N. REDDY, "Mechanics of Bimodular Composite Structures", in "Mechanics of Composite Materials: Recent Advances", Proceedings of the IUTAM Symposium, VPI (Blacksburg, Virginia, 1982) pp. 323–37.
42. P. H. PETIT and M. E. WADDOUPS, *J. Compos. Mater.* **3** (1969) 2.
43. C. C. CHAMIS, *SAMPE Q.* **15** (1984) 14.
44. "Modern Plastics Encyclopedia" (Engineering Data Bank, McGraw-Hill, New York, 1983).
45. C. M. KUO, K. TAKAHASHI and T. W. CHOU, *J. Compos. Mater.* **22** (1988) 1004.
46. S. Y. LUO and T. W. CHOU, *J. Appl. Mech.* **55** (1988) 149.
47. R. S. RIVLIN, "Networks of Inextensible Cords", in Nonlinear Problems of Engineering" (Academic, New York, 1964).
48. A. E. GREEN and J. E. ADKINS, "Large Elastic Deformations" (Oxford University Press, London, 1970).
49. H. T. HAHN and S. W. TSAI, *J. Compes. Mater.* **7** (1973) 102.
50. K. TAKAHASHI and T. W. CHOU, *J. Compos. Mater.* **21** (1987) 396.
51. R. S. JONES and MORGAN, H. S., *AIAA J.* **15** (1977) 1669.
52. PIPKIN, A. C., "Finite Deformation in Material Reinforced With Inextensible cords", in "Finite Elasticity", edited by R. S. Rivlin (ASME, New York, 1977) pp. 91–102.
53. Y. C. FUNG, "Foundations of Solid Mechanics" (Prentice-Hall, Englewood Cliffs, 1965).
54. AZAR-DOKHT PARVIZI, PhD dissertation, University of Surrey (1978).
55. S. Y. LUO and T. W. CHOU, to be published.

Received 19 April
and accepted 19 May 1988